DESIGN, DEVELOPMENT AND FORCE CONTROL IMPLEMENTATION FOR A WEARABLE EXOSKELETON WITH HIGH POWER-TO-WEIGHT RATIO

A Thesis

by

Mustafa Derman

Submitted to the
Graduate School of Sciences and Engineering
In Partial Fulfillment of the Requirements for
the Degree of

Master of Science

in the
Department of Mechanical Engineering

Özyeğin University
June 2023

DESIGN, DEVELOPMENT AND FORCE CONTROL IMPLEMENTATION FOR A WEARABLE EXOSKELETON WITH HIGH POWER-TO-WEIGHT RATIO

Approved by:

Asst. Prof. Barkan Uğurlu, Advisor
Dept. of Mechanical Eng.
Özyeğin University

Asst. Prof. Özkan Bebek
Dept. of Mechanical Eng.
Özyeğin University

Asst. Prof. Yeşim Öniz
Dept. of Mechatronics Eng.
İstanbul Bilgi University

Date Approved: 23 May 2023

To my family...

ABSTRACT

Physical rehabilitation has a crucial role in the recovery and preservation of physical function, mobility, and overall health after an injury or disability. Exoskeletons can serve as useful tools in physical rehabilitation by providing a safe and controlled environment for patients to perform functional movements. This thesis proposes a design methodology and validation processes for a lower body exoskeleton with active hip, knee, and ankle joints. Four different designs were presented and qualitatively compared their joint range, torque controllability, weight, and wearability. Using a human-robot coupled simulation model, actuator torques and loading on mechanical links were obtained. The final design was evaluated in the MSC Adams environment concerning two different dynamic motions. Subsequently, the exoskeleton was manufactured and assembled after the final design was verified. To verify the locomotion methods, a robot model constrained in the sagittal plane was created using the RaiSim simulator. The dynamic model of the exoskeleton was calculated using the Lagrangian method, and CTC was also applied. Various controller methods were implemented to validate the exoskeleton and the SEAs, and their position-tracking performances were compared. Furthermore, the torque controllability of the actuator was verified.

ÖZETÇE

Fiziksel rehabilitasyon, bir yaralanma veya sakatlıktan sonra fiziksel fonksiyonların, hareketliliğin ve genel sağlığın iyileştirilmesi ve korunmasında önemli bir rol oynamaktadır. Dıs iskeletler, hastaların fonksiyonel hareketlerini gerçekleştirmeleri için güvenli ve kontrol edilebilir bir ortam sağlayarak fiziksel rehabilitasyonda yararlı bir araç olarak kullanılabilirler. Bu tez, aktif kalça, diz ve ayak bileği eklemleri olan bir alt gövde dış iskeleti için tasarım metodolojisi ve doğrulama süreçleri önermektedir. Dört farklı tasarım sunulmuş ve eklem hareket aralığı, tork kontrol edilebilirliği, ağırlık ve giyilebilirlik açısından nitel olarak karşılaştırılmıştır. İnsan-robot eşleştirilmiş simülasyon modeli kullanılarak eyleyici torkları ve mekanik bağlantılara binen yükler elde edilmiştir. Son tasarım, iki farklı dinamik hareket açısından MSC Adams ortamında değerlendirilmiştir. Tasarım doğrulandıktan sonra, dış iskelet üretilmiş ve montajı gerçekleştirilmiştir. Lokomasyon yöntemlerini doğrulamak için, RaiSim ortamında sagittal düzlemde kısıtlanmış bir robot modeli oluşturulmuştur. Dış iskeletin dinamik modeli Lagrange yöntemi kullanılarak hesaplanmış ve CTC'de uygulanmıştır. Çeşitli kontrolcü yöntemleri, dış iskelet ve SEA'ların pozisyon takibi performanslarını doğrulamak için uygulanmış ve karşılaştırılmıştır. Ayrıca, eyleyicilerin tork kontrol edilebilirliği doğrulanmıştır.

ACKNOWLEDGEMENTS

I would like to thank my thesis advisor, Asst. Prof. Barkan Ugurlu, for giving me the opportunity to use all these resources and for his guidance throughout my M.Sc. study. I also would like to thank my professors Asst. Prof. Ozkan Bebek and Asst. Prof. Ramazan Unal for their support.

I would like to express my gratitude to my greatest supporters, my family and Hazal Çelik, for their unwavering encouragement throughout my M.Sc. journey.

Lastly, I wish to thank to my colleagues who worked alongside me on this project: Süleyman Can Çevik and Alihan Kuru. Additionally, I am grateful for the support of my friends in the laboratory: Ahmed Fahmy Soliman, Altun Rzayev, Barış Baysal, Burak Özkaynak, Deniz Yılmaz, Dilay Yeşildağ, Ege Gediksiz, Erim Can Özçınar, Mehmet Can Yıldırım, Sinan Coruk, Sinan Emre, Tuğçe Ersoy and Omid Khosrowshahi.

This work is supported by the Scientific and Technological Research Council of Turkey (TUBITAK), with the project 118E922.

TABLE OF CONTENTS

LIST OF TABLES

LIST OF FIGURES

List of Abbreviations

SCI Spinal Cord İnjury

F/E Flexion/Extension

D/PF Dorsi/Plantar Flexion

A/A Adduction/Abduction

COM Center of Mass

DOF Degree of Freedom

SEA Series Elastic Actuator

EM Electromagnetic Motor

CAD Computer-Aided Design

DOB Disturbance Observer

PID Proportional-Integral-Derivative

FF Feed-Forward

ZMP Zero Moment Point

CTC Computed Torque Control

RMS Root Mean Square

CHAPTER I

INTRODUCTION

Physical rehabilitation has a crucial role in the recovery and preservation of physical function, mobility, and overall health following an injury. It can aid in muscle strengthening, reduce joint stress, enhance balance, alleviate joint discomfort, and even prevent potential injuries [1, 2, 3]. Physical rehabilitation can be necessary for any medical condition that impacts the nerves, muscles, bones, or brain, leading to either temporary or permanent disability.

SCI is one of these conditions that occurs because of the damage to the spinal cord, disabling the communication between the brain and body. SCI can have a significant impact on an individual's daily life. Nevertheless, patients can recover from this condition with appropriate rehabilitation [4]. Although there is evidence stating the efficacy of body-weight supported training for improving walking ability in individuals with SCI, the repetition number poses a constraint on the clinical implementation of this treatment, as therapists are unable to excessively repeat identical movements. Development of robotics devices which provides automated medical assistance may improve the quality of treatment and lighten therapists' weight [5]. Medical robotic devices include various types of machines and equipment such as exoskeletons.

Exoskeletons can be used as a tool for physical rehabilitation by providing a safe and controlled environment for patients to practice walking and performing functional movements. To corroborate this, Zeilig et al. conducted a study that demonstrated the effectiveness of lower-limb exoskeletons in improving walking speed, endurance, and balance in individuals with SCI, as compared to conventional gait training [6]. Similarly, a systematic review conducted by Lu et al. showed that exoskeleton-assisted gait training can enhance balance in patients with stroke [7]. Moreover, the use of lower-limb exoskeletons may result in psychological benefits for patients, including improvements in patient's psychology and overall quality of life [8, 4]. These findings suggest that exoskeletons hold great potential as a tool for physical rehabilitation, promoting greater mobility, independence, and well-being in individuals with impairments.

Nevertheless, some studies mention the lack of scientific evidence to show the positive effect of the lower body exoskeletons, and more information about long-term performance should be stated [9, 10, 11]. These studies focused on several commercial exoskeletons and their published results to evaluate their usefulness. In order to enhance the exoskeleton concepts and solve their issues, researchers continue to develop different designs.

Considering the advantages of exoskeletons to the medical world, this study focuses on lower body exoskeleton design methodology and its locomotion implementation for rehabilitation purposes.

1.1 Lower Body Exoskeleton - State-of-the-art

Lower body exoskeletons have the potential to change daily life for individuals, especially those with ambulatory issues. In particular, they could be valuable assets to improve the quality of physiotherapy and positively impact the condition of life [12, 13]. Some achievements of the exoskeletons in rehabilitation are decrease in pressure wound, improving circulatory function and regaining the ability to walk [14]. To that end, several lower body exoskeleton systems have been developed and benefited by many SCI patients [15].

Conventional lower body exoskeletons have two active joints per leg, providing active assistance through knee and hip F/E axes [16, 17]. This joint configuration allows the user to swing her/his leg forward with the least number of active joints possible. Various design architecture was proposed to improve the performance of conventional *2-active-joints-per-leg* exoskeletons. For instance, Lee et al. developed an assistive device in which hip and knee actuators were placed at the back of the hip, and the actuators were connected to the joints via a pulley system [18]. Since elderly people have difficulties while walking and standing, the device was designed to support the movements and reduce the torque needed for the joints. Similarly, Sado et al. designed an assistive exoskeleton for handling heavy loads in which hip and knee joints are powered via motors directly [19].

While the conventional design approach may reduce the cost, weight, and energy consumption, it requires the user's upper body power to maintain static balance with the help of crutches. The lack of active support at the ankle joint significantly limits the gait capability of exoskeletons, and users need large upper body engagement [20, 21]. Furthermore, using crutches for a long time to stay in balance causes pain on arms joints especially on shoulder [22, 23, 24].

Increasing the number of active joints may tackle this issue [25]. With the addition of an active ankle joint along the D/PF axis, self-balancing in the sagittal plane could be achieved [26]. There are several exoskeleton designs available which contains 3 active DOFs aiming various purposes. Exoskeletons that aim to compensate the user's effort utilizes compact actuators thus, they generally have limited torque output [27]. Therefore, they require human assistance in order to stay in balance along the sagittal plane even though they have the required kinematic design. Meanwhile there are other medical exoskeletons focusing on rehabilitation and paraplegic patients, that have to support the weight of robot and the patient. Therefore, actuators have to supply higher torques to each joint in order to stand [6].

Furthermore, to shift the COM laterally, an active joint along the A/A axis can be added [28, 29, 30]. With the addition of even more active joints, fully actuated systems that deliver hands-free 3-D walking support can be demonstrated [31, 32].

To enhance the design of exoskeletons, it is possible to employ a simulation environment as a preliminary step before conducting experimental trials. Mo et al. introduced a framework based on simulations, which enables the evaluation of an already-existing exoskeleton in terms of efficiency, and subsequently, the optimization of its design based on the obtained results [33]. A comparable procedure of design based on simulations can be employed prior to production, leading to potential reductions in manufacturing processes and costs.

While adding more active joints improves the motion capability of lower-body exoskeletons, their mechanical design becomes more complicated. Notably, the actuator placement is an important challenge since these systems must be wearable. Considering these trade-offs, 3 DOFs per leg is aimed for the design to create a system which can support the weight of the exoskeleton and the user meanwhile being simple and easily wearable.

1.2 Aim of the Thesis

This thesis provides a design methodology for a lower body exoskeleton with active hip, knee, and ankle joints. To that end, four distinct designs were proposed and qualitatively compared; using a human-robot coupled simulation model, actuator torques and loading on mechanical links were obtained. Assessing the static and dynamic loading data, robot links were further optimized for mass reduction. The final design was evaluated in a simulation environment concerning stand-to-sit and dynamic walking motion capabilities. Furthermore, different controller methods are implemented to validate the exoskeleton and its torque controlled actuator unit, and the position-tracking performances are evaluated.

CHAPTER II

MECHANICAL DESIGN

The addition of active joints improves motion flexibility, although it may lead to heavy and bulky designs. Working around this trade-off, a system that can provide assistance to hip, knee, and ankle joints, along the F/E and D/PF axes, respectively, is aimed for our design. Therefore, we can ensure complete balancing along the sagittal plane, the dominant motion plane for walking [26, 34]. In Fig. 1, an initial conceptual design and its simulation model are displayed. Exoskeleton leg links are aimed to be user-specific and easily replaceable; thus, different heights of human models can be used in the simulation.

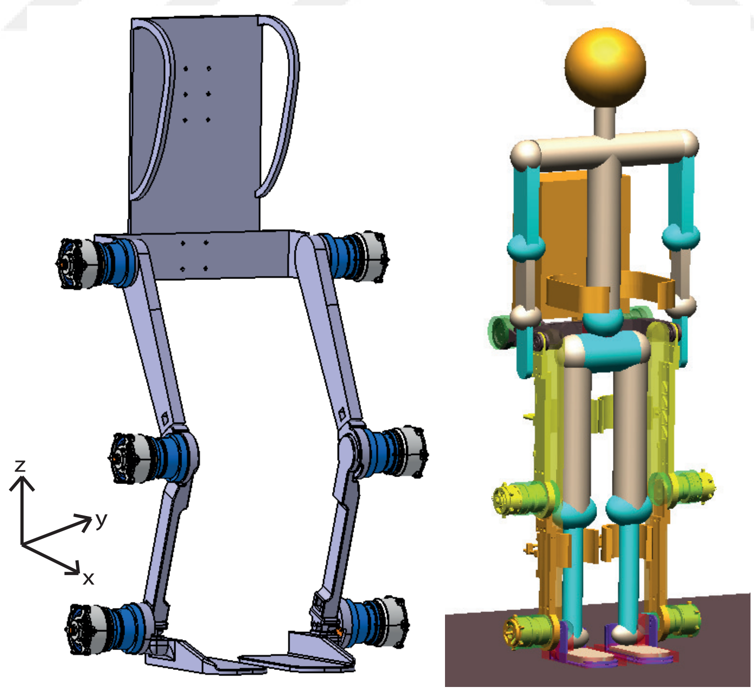

Figure 1: Left: An Initial conceptual design of the lower body exoskeleton. The x-z plane is the sagittal plane Right: Human-robot coupled simulation model in MSC ADAMS. Weight and CoM are not affected by the visual shells added onto exoskeleton body parts.

2.1 Range of Motion

It is argued that the joint ranges of an exoskeleton should match with average human joint ranges in the sagittal plane. Referring to Roass and Andersson's study in [35], the mean values concerning average healthy human joints ranges are given in Table 1, with standard deviations in parentheses.

Table 1: Joint range data for hip, knee, and ankle.

Joint	Motion	Right Limb (degrees)	Left Limb (degrees)
Hip	Extension	9.4 (5.3)	9.5 (5.2)
	Flexion	120.3 (8.3)	120.4 (8.3)
Knee	Extension	143.8 (6.4)	143.7 (6.6)
	Flexion	1.6 (2.8)	1.7 (3.0)
Ankle	Dorsiflexion	15.3 (5.8)	15.3 (5.8)
	Plantar Flexion	39.7 (7.5)	39.6 (7.7)

From a safety point of view, the robot joints should not exceed the human joint ranges. Accordingly, the following joint ranges in our design are aimed with a safety margin of 10% less than the average values in mind:

- Hip Flexion/Extension: $\sim 108°/\sim 5°$
- Knee Flexion/Extension: $\sim 0°/\sim 130°$
- Ankle Dorsi/Plantar Flexion: $\sim 13.5°/\sim 36°$

2.2 Design Iterations for Actuator Placement

Four different designs were conducted for actuator placements.

2.2.1 Higher CoM Height and Reduced Leg Inertia

In Fig. 2-a, all the actuators were placed as high as possible to keep the center of mass close to the upper body. In doing so, the leg inertia concerning the hip joint could be reduced. Furthermore, the system may approximate the inverted pendulum

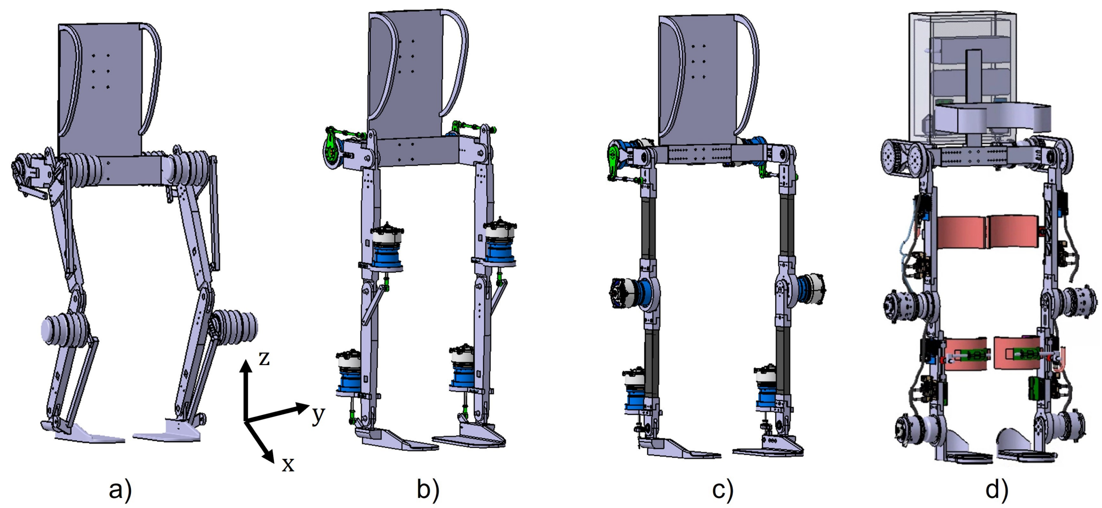

Figure 2: Iterations on Designing the Exoskeleton a) 4-bar based design b) Vertically placed actuators c) Knee actuator direct placement d) Ankle actuator direct placement, braces, and electronics added only as visual without any mass

model, potentially facilitating more feasible balance control strategies [29, 36]. With this goal in mind, hip and knee motors were deployed at the waist area while the ankle motor was placed at the knee area. Actuator torques were transmitted to joints via lever arms. However, when the actuators are gathered around the waist area, we assess that the wearability aspect of the system could be deteriorated and addition of linkage parts could increase the mass and the possibility of backlash.

2.2.2 Vertically Placed Knee and Ankle Actuators

To improve the wearability of the system, it is essential to open the front area of the exoskeleton. To this end, a design has been studied in which the motors are placed vertically, and the force is transmitted by ball screw mechanisms; see Fig. 2-b. Thus, the system will be lightened by eliminating long, force transmission parts, and the anterior region of the exoskeleton will be opened at a level that would allow the user to wear the system relatively easily. On the contrary, the vertical positioning of the knee actuators made it challenging to provide the necessary range of motion to the knee joint by using a ball screw and a lever arm. In order to overcome this issue, the length required for the screw shaft has been reduced by tilting the knee motors. Despite these efforts, this design was deemed insufficient since an extended ball screw mechanism is required to ensure the target range of motion concerning the knee joint.

2.2.3 Vertically Placed Ankle Actuator

In an effort to ensure the target knee joint range and remove the extra loading due to torque transmission mechanisms, a direct actuator placement was considered concerning the knee joint; see Fig. 2-c. In this design, the ankle joint was also placed vertically at the calf area for a more compact design. The main problem in this approach is the non-backdrivability of the ball screw mechanism. Therefore, even if the actuator unit is torque-controllable, the non-backdrivability of the transmission mechanism prevents the torque controllability of the ankle joint and increases the complexity of the design [37].

2.2.4 Directly Driven Ankle and Knee Joints

The torque controllability aspect of the exoskeleton is one of the main essential features when considering safe and dependable physical human-robot interaction [38]. Thus, the ankle actuator was also directly attached to the joint; see Fig. 2-d. Only the hip joint was placed at the back of the waist area to simplify the structure. The 4-bar design at the hip joint dramatically reduces the effective joint range. To remedy this issue, a pulley-belt system is implemented concerning the hip joint.

Table 2: Comparison of total mass and dominant axis leg inertias for each actuator configurations

		Leg Inertias [kgm^2]	
Exoskeleton Configuration	Mass [kg]	Iox	Ioy
1) Higher CoM	38.438	3.012	3.058
2) Vertical Placed Knee	38.362	3.655	3.694
3) Vertical Placed Ankle	35.881	3.455	3.465
4) Direct Drive Knee and Ankle	35.422	3.464	3.456

In Table 2, total mass and leg inertiae of different designs are tabulated. The leg inertia of the first design is lower because the actuator masses are closer to the hip joint. However, to achieve this configuration, extra mechanisms should be added; thus, total mass increases.

In conclusion, even though having the actuators above the joint area reduces the leg inertia, it increases the total weight and potentially hampers the wearability. Although, using a ball-screw system might improve wearability, non-back drivability prevents torque controllability. Thus, having reviewed a series of leg architectures with distinct actuator placement strategies, the design in Fig. 2-d was deemed to be a suitable choice for weight reduction, joint range, torque controllability, and wearability.

2.3 Simulation-based Exoskeleton Design

We aim to optimize the exoskeleton design using the simulation with the human-exoskeleton coupled model before production [33].

Once a final design concept was obtained, simulation studies were conducted to finalize the design process regarding the actuator selection and topology optimization. For this purpose, a coupled human-exoskeleton model was constructed in the MSC ADAMS environment [25], and the motion is constrained in the sagittal plane. Two different simulation scenarios were considered: i) stand-to-sit motion, ii) dynamic walking motion.

2.3.1 Actuator Selection

Torque controllability is an important factor when assessing the enhanced physical interaction capabilities of the exoskeletons [38]. To this end, the series elastic actuator architecture proposed in [37] is adopted.

Assessing the joint torque variations obtained via simulation, the most significant torque demand is observed at the knee joint. For stand-to-sit motion, a maximum

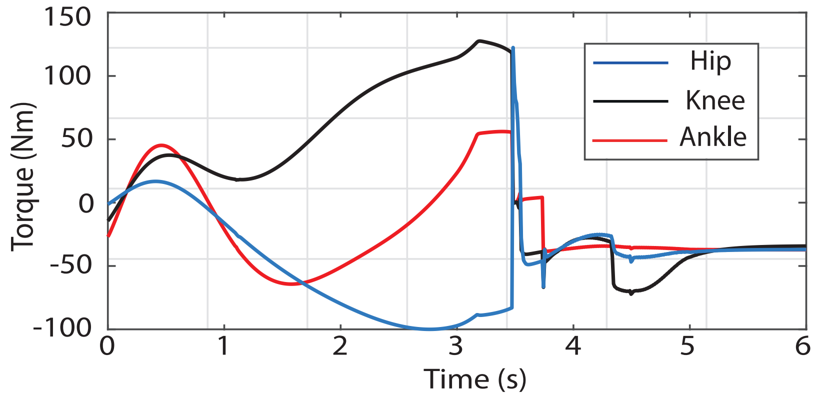

Figure 3: Hip, knee, and ankle torques while performing the stand-to-sit motion.

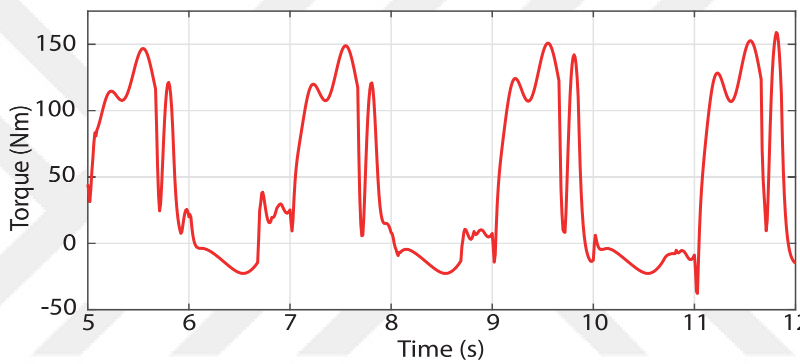

Figure 4: Knee torque during dynamic walking at 0.2 m/s

of 130 Nm torque requirement was observed; see Fig. 3. During walking, a torque demand up to 150 Nm was observed; see Fig. 4. Meanwhile, hip and ankle joints have relatively more conserved torque demand, which does not exceed 100 Nm; see Fig. 5.

With these results in mind, two different SEA units were considered; see Table 3. Frameless brushless motors (Kollmorgen TBM-7615 for the hip and ankle and Kollmorgen TBM-7631 for the knee) were employed for reduced weight, coupled with strain wave gears (Harmonic Drive CPL-25A) with a 100:1 ratio. Two absolute encoders with a resolution of 18-bit (FENAC FNC 40HFS 8S1630V-R2) were utilized to measure the link and motor position separately. A custom-made torsional spring was placed between the gear output and mechanical output [37].

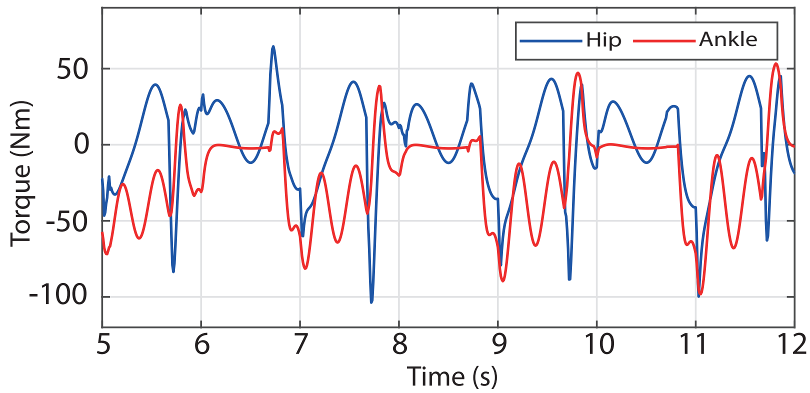

Figure 5: Hip and ankle torques during dynamic walking at 0.2 m/s

Table 3: Basic properties of SEA units.

	Knee SEA	Hip & Ankle SEA
Maximum Cont. Torque (Nm)	169	94.4
Weight (kg)	2.55	2.15
Spring Stiffness (Nm/deg)	80	40
Radius-Length (mm x mm)	47x168	47x147
Torque-Mass Ratio (Nm/kg)	66.27	43.9

2.3.2 Finite Element Analysis and Topology Optimization

In order to lower the weight of the exoskeleton, we implemented stress analyses on each part so that the link topologies could be optimized. The maximum loads acting on the joints were used, i.e., 160 Nm for the knee joint, obtained from the simulation data. Static structural analysis was applied by fixing one end of the part and applying torque to the other using Ansys. Following the Von-Mises stress results, we could determine the areas with the lowest stress concentration.

Since thigh and shine links are relatively longer, they may be subject to buckling. To this end, calculating the critical unit load for the case of central loading is necessary. The critical unit load can be described below:

$$P_{cr}/A = Cpi^2 E/(l/k)^2 \tag{1}$$

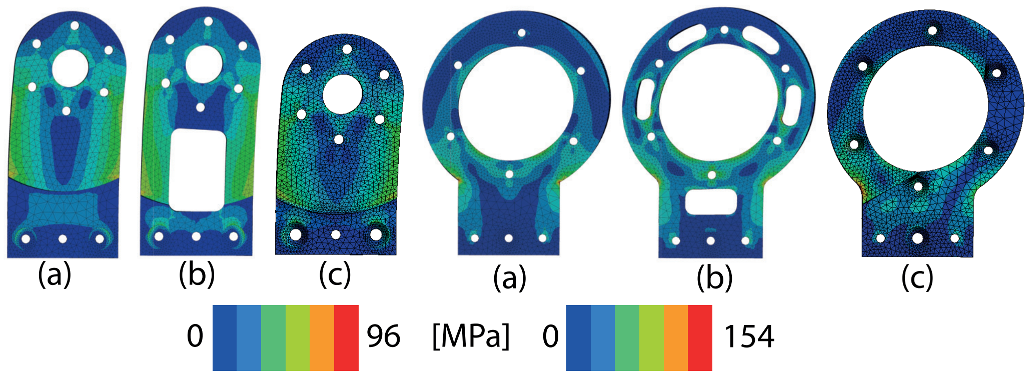

Figure 6: Topology optimization for the knee motor link and actuator base. a) Initial stress analysis before the optimization b) Emptied link after the topology optimization c) Mechanical limits added after topology optimization.

The ratio P_{cr}/A represents the critical unit load, l/k is called the slenderness ratio, E is Young's Modulus, and C is the constant used to determine the column type. Maximum load occurs when the exoskeleton is at a single support phase. In this case, we may assume the link's bottom base is fixed, and its top is free, hence $C = 1/4$ [39].

Topology optimization was performed by respecting the Von-Mises stress results and connection constraints. The retained volume percentage was given as 50% as an objective. In accordance with the topology optimization result, certain removable regions were specified. Afterward, the link in question was redesigned to be easily manufacturable while those regions can be removed from the design. Furthermore, a follow-up stress analysis was performed to guarantee that the mechanical structure can withstand maximum loading while the increased deformation due to topology optimization is negligible. Two exemplary topology optimization results can be viewed in Fig. 6 for the knee motor link and actuator base.

2.3.3 Stand-to-Sit Motion

To generate stand-to-sit motion, joint trajectories were generated using higher-order polynomials to satisfy initial and final constraints. In Fig. 7, four significant moments

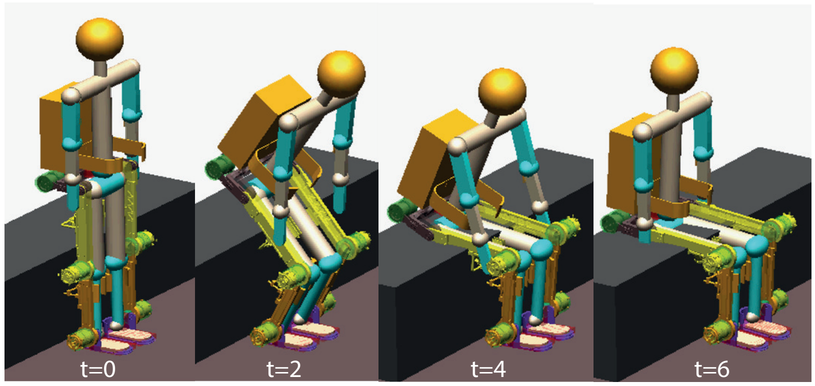

Figure 7: Animation of motion from stand to sit. In the third scene, the exoskeleton contacts the chair.

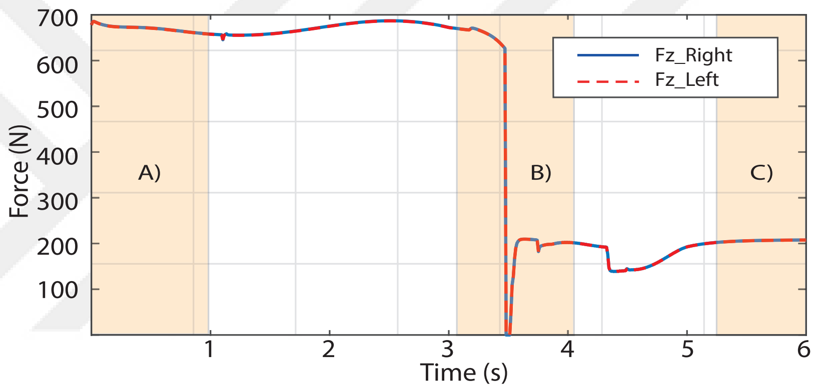

Figure 8: Ground reaction force acting on each foot during stand-to-sit motion. A) standing, B) contacting with the chair C) sitting straight

can be viewed. Moreover, Fig. 8 displays the vertical ground reaction forces during stand-to-sit motion. As may be observed, the measured vertical forces were decreased to a certain extent when the human-robot combined system successfully achieved sitting.

2.3.4 Dynamic Walking

In order to check the feasibility of the proposed design, a detailed walking simulation experiment was carried out. Walking parameters are assigned as follows: single and double support periods were 0.7 and 0.3 s, the maximum foot clearance was 4 cm, the stride length was 47.8 cm, and the target forward velocity was 0.2 m/s. The novel controller proposed in [25] was employed to ensure robust locomotion behavior.

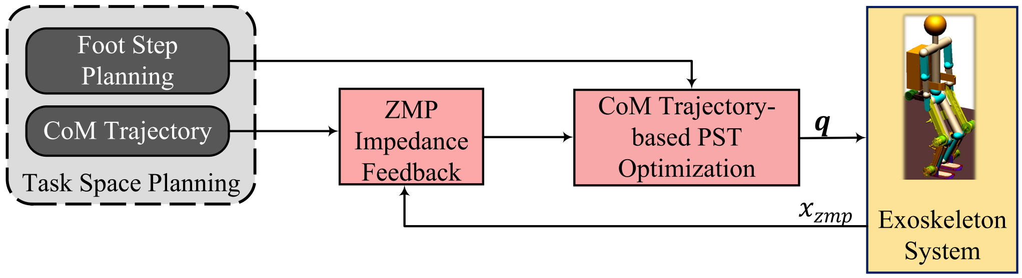

Figure 9: Block diagram of the control system. ZMP represents the zero moment point, PST stands for a prioritized stack of tasks and q is joint angles of the exoskeleton

Its simplified block diagram can be viewed in Fig. 9. The main feature of this controller is the ability to suppress perturbations due to parameter uncertainty; it does not require any information regarding the human user except the total weight and height. Human legs are connected to the exoskeleton via parallel joints, and the foot is fixed to the exoskeleton, i.e., the human thigh is parallel to the exoskeleton thigh.

In Fig. 10, CoM position and feet position were plotted [17]. Due to the presence of human model, the CoM projection is slightly shifted forward. Nevertheless, we can observe that the locomotion pattern is symmetric and forward velocity is steady. In Fig. 10, x-axis ZMP is depicted. As may be examined in this figure, the ZMP response is always within the support polygon, adequately validating the dynamic balance throughout the whole walking period. Finally, joint angle variations are plotted in Fig. 11, indicating that they are all within the specified joint ranges.

2.4 Finalization of the Mechanical Design

After gathering the results from the simulations, exoskeleton design was revised and finalized. During the simulation studies for stand-to-sit and walking movements, the range of motion of the exoskeleton joints and the mean values obtained from healthy individuals are as indicated in the table below:

Mechanical limits were designed for the joints, by taking into account the human

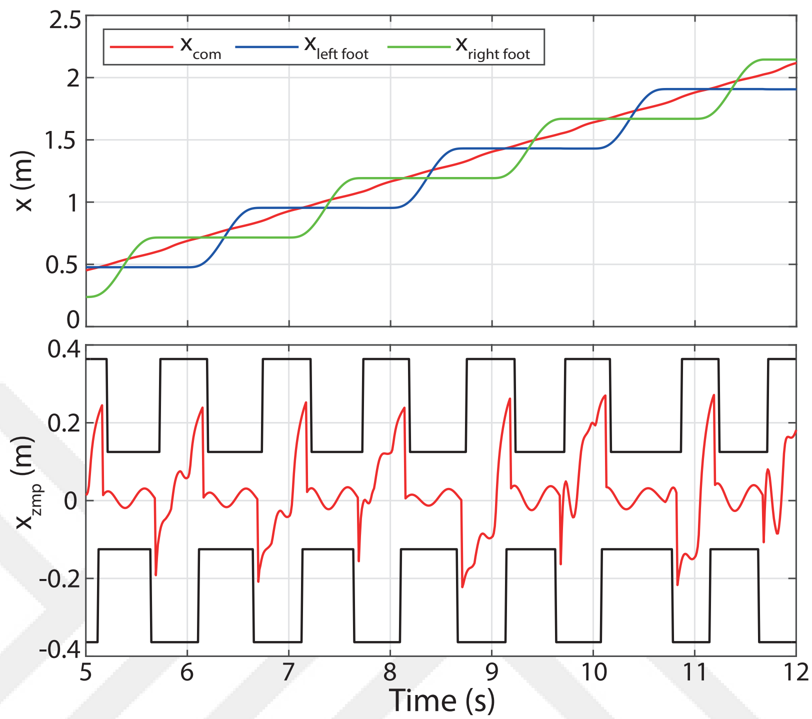

Figure 10: 1) Trajectories of the CoM and both feet. 2) x-axis ZMP trajectory in the local coordinate frame, together with the support polygon.

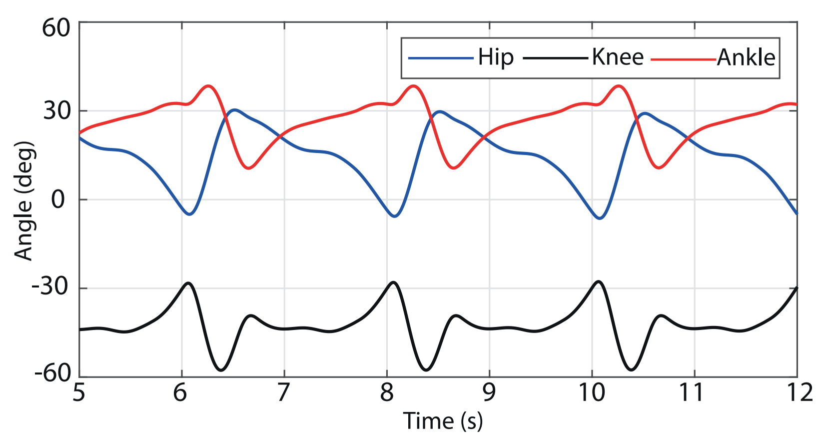

Figure 11: Joint angle trajectories throughout the entire walking period.

Table 4: Joint ranges of motion comparison of healthy individuals and the simulation

Joint	Data from Boone and Azen (1979)	Walking Simulation	Sit-to-Stand Simulation
Hip			
Flexion	120.3 (8.3)	35	130
Extension	9.5 (5.2)	7	0
Knee			
Flexion	1.6 (2.8)	0	0
Extension	143.8 (6.4)	65	90
Ankle			
Dorsi Flexion	15.3 (5.8)	0	30
Plantar Flexion	39.7 (7.5)	45	0

joint ranges and the values obtained as a result of the simulation. Thus, the joints of the system could be prevented from moving in a way that may harm users.

Table 5: Range of motions of the exoskeleton constrained within the mechanical limits

Joint	Joints Range of Motions
Hip	
Flexion	120
Extension	10
Knee	
Flexion	0
Extension	120
Ankle	
Dorsi Flexion	15
Plantar Flexion	45

The mechanical limits for the knee and ankle joint are designed on the actuator caps. When the motor link reaches the movement limit, it will hit the actuator cap and the link will not move any further. Mechanical limits are shown on the CAD model in Fig. 12.

The parallelogram design used previously at the hip joint allows the actuator to

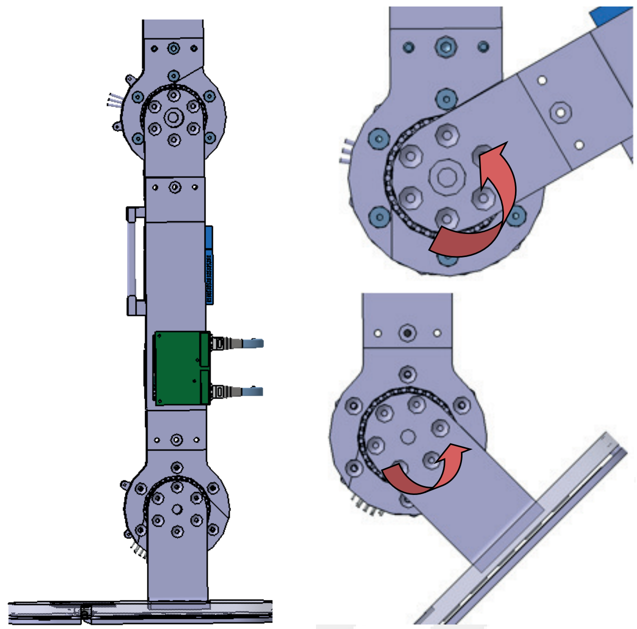

Figure 12: Mechanical limits designed for knee and ankle joints

be placed behind the user's waist. Although it provides the necessary range of motion for walking, when the hip joint reaches an angle of 90 degrees, the connectors used in the parallelogram design collide and restrict the movement, so the sitting action cannot be performed. For this reason, the parallelogram design had to be abandoned, and the moment should be transmitted to the hip joint by a different mechanism. On the other hand, direct insertion of actuators has been avoided to prevent hitting the seat or chair arms while sitting.

In order to preserve the placement of the actuators, the parallelogram connection links was removed, and a special model belt-pulley system was designed instead. T profile belts are not strong enough to withstand the force produced by the 94.4 Nm moment which hip actuator supplies. To endure against high torque values, the belt model should be reinforced with steel wires, and at the same time, its backlash should be as low as possible. In order to meet these needs, belt models in different profiles were investigated, and it was decided that the AT profile belts were the most suitable model for our needs. The maximum force acting on the belts was obtained using eq.

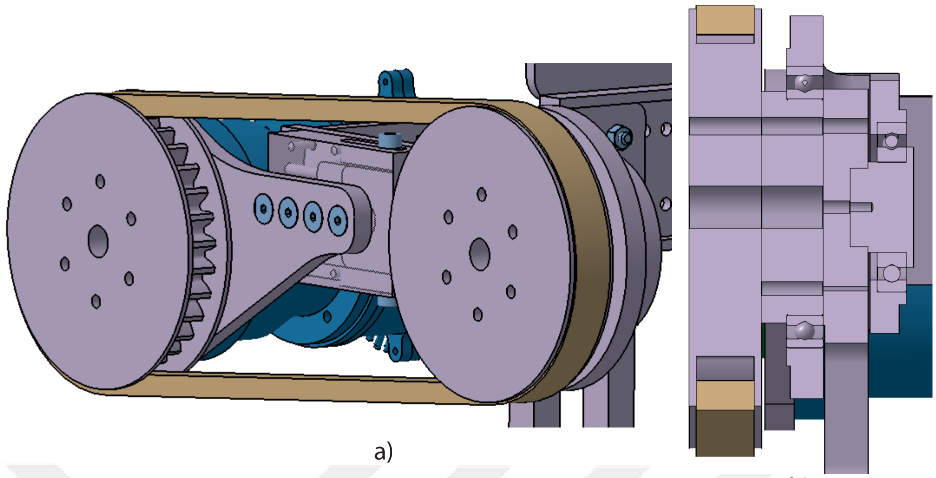

Figure 13: a)Hip joint design and b)Cross-section of the hip joint

(2).

$$F_u = \frac{2(M_{output})(10^3)}{d_{w2}} \tag{2}$$

F_u is the force acting on the belt, M_{output} is the moment given to the pulleys, and d_{w2} is the pulley diameter. In this case, the highest forces to occur in different pulley diameters were calculated, and a search was done for the belt in the width and profile suitable for our needs. 16 mm wide belts with AT10 profile and 100 mm diameter pulleys were used. Mechanical design after revision is given in Fig. 14.

2.5 Manufacturing and Assembly

Aluminum block materials were ordered from the supplier and CNC machining process was held in the manufacturing laboratory in Ozyegin University. Parts that do not need CNC machining were sent to water jet and laser cutting companies to be manufactured. 3D printers were used to produce parts that do not carry any weight. Link distants, circuit holders, brace rail bases, electronic component rails etc. were manufactured from PLA, Onix and ABS materials using 3D printers available

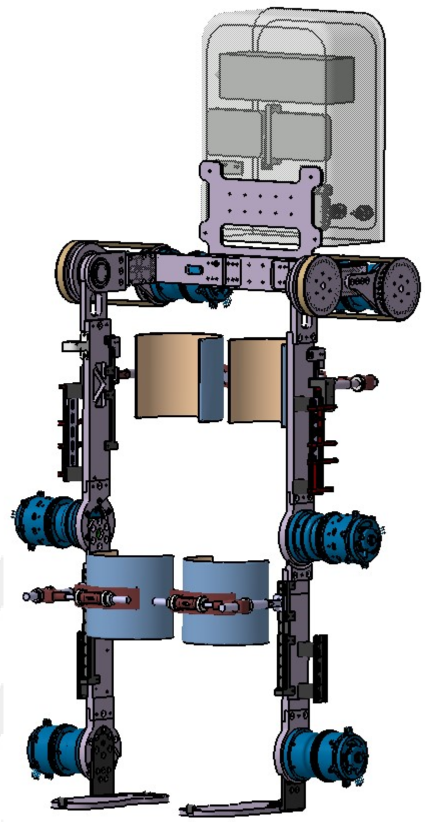

Figure 14: Revised final design after the simulation results

in Robotics and Biomechatronics laboratories in Ozyegin University. Certain commercial off-the-shelf products, such as electric box, belt-pulley systems, linear rails employed in human brace system were utilized and placed directly on the exoskeleton.

Mounting and fixations were done with screws so that they can be replaced or modified later if necessary. In order to be adjusted for each user easily, leg links were attached to the actuator bases using only three screws on each end.

Once SEA tests and controller experiments were completed, the exoskeleton fully assembled. The human connection braces were not mounted to the exoskeleton during the experiments, as they would wobble when attached to the exoskeleton. A platform was designed and manufactured so that the exoskeleton could be tethered and lifted up using a crane during experiments or studies. Tests can be carried out in the air without placing the exoskeleton on the ground. Assembly of the mechanical parts and electronic connections of exoskeleton and human dummy can be seen in Fig. 15.

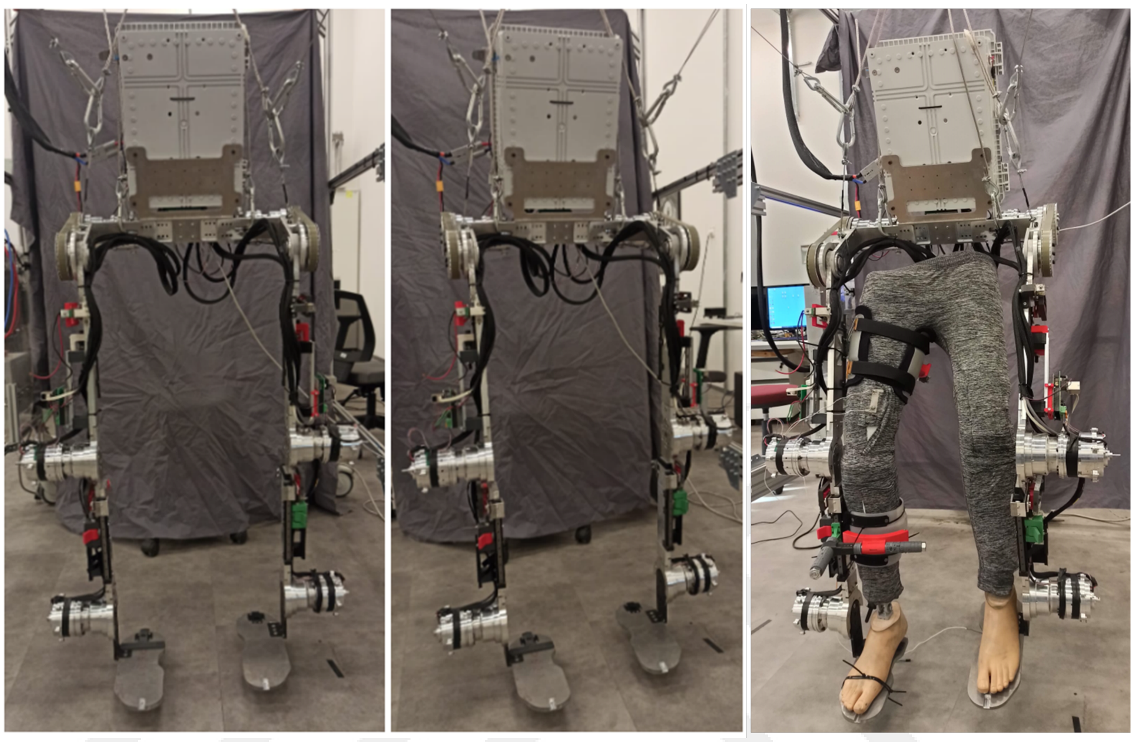

Figure 15: Assembly of the lower body exoskeleton and human dummy placed using braces

2.6 Electronics Design

Electronic components of the exoskeleton were gathered considering the power requirement and the control/sensor systems of the robot. The total electronic system diagram of the exoskeleton is shown in Fig. 16.

As the main controller of the exoskeleton, NVIDIA Jetson AGX Xavier was selected. The main consideration for the communication was to be fast so that the control would be more efficient. Therefore, whole communication of the robot was done using EtherCAT system while Xavier was the master and the motor drivers were the slaves. In order to read the motor and link positions, high resolution absolute rotary encoders were used. While motor driver was reading the motor encoder, a custom made EtherCAT shield circuit was used for the link encoder. EsmaCAT's A/D

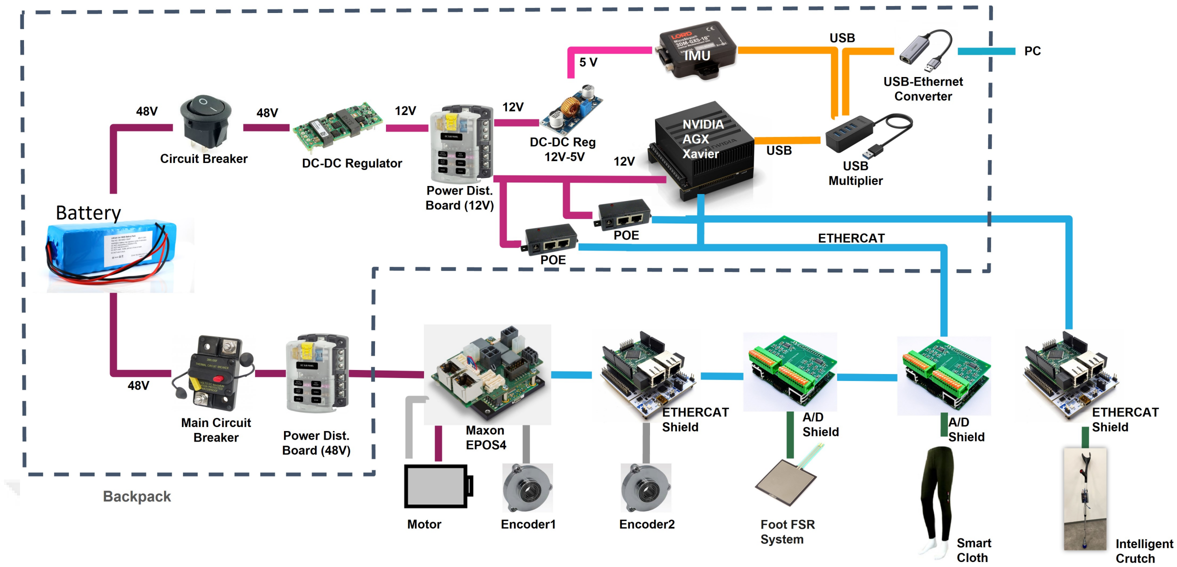

Figure 16: Electronic system diagram of the exoskeleton

shield circuits were also added to the communication so that the sensorized shoe and the smart cloth sensors could be implemented. In pursuance of minimizing the cable, some of the electronic parts were placed at the legs of the exoskeleton. Since the EtherCAT communication needs a chain connection, Ethernet cables were extended from legs to the backpack.

CHAPTER III

CONTROLLER IMPLEMENTATION

3.1 Series Elastic Actuator

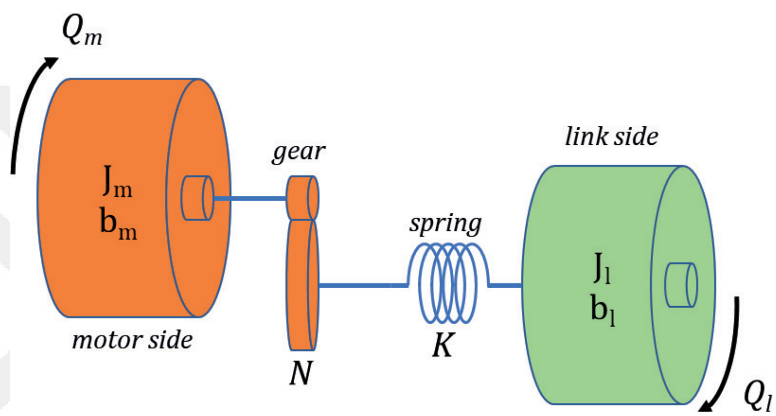

Figure 17: Simplified mechanical SEA plant model

Generally, SEAs consist of three parts; an EM, a reduction gear, and an elastic element. The purpose of using reduction gears is to increase the torque output since EMs operate at high velocity with low torque output. However, implementation of reduction gears creates some disadvantages like internal friction and backlash [40]. Furthermore, introducing a gear increases the reflected inertia by the square of the gear ratio and back-driveability of the actuator is being reduced; therefore, external forces may damage the actuator.

To overcome this issue, an elastic material is added between the gear and the output link of the system which has the potential to mitigate the peak torques, and enables implementation of high-fidelity force control [41]. The closed-loop force control of the SEA can be achieved by utilizing the relationship between the spring deflection and the torque output of the actuator. Hence, without using force sensors, the force control problem can be converted to a position control problem by only measuring the spring deflection using the rotary encoders. Various exoskeletons are powered via SEAs such as; Mindwalker [28], Symbitron [30], Mina v2 [17], and Co-Ex [29]. While the concept of SEA is generally the same, different designs are proposed in the literature [42, 43, 44]. In Fig. 17, a simplified mechanical model of the SEA is represented.

SEA is a system which has two inertiae components connected with a torsional spring element. The motor side is the first inertia and the link side is the second inertia. In order to increase the output torque, a gear element can be used in between the motor side and the spring. The spring deflection can be measured and converted to torque using a pair of encoders, so that the torque control problem can be treated as a deflection problem [45]. Formulation of the spring deflection is

$$\tau_l = KQ_d = K(\frac{Q_m}{N} - Q_l) \tag{3}$$

where τ_l is the link torque, K is the spring constant, Q_d is the spring deflection, N is the gear ratio, Q_m and Q_l are motor and link positions respectively.

3.1.1 SEA Model in Laplace Domain

Block diagram of the SEA can be created in Fig. 18. Since there are 2 different inertiae components, motor and link sides transfer functions can be represented as shown below, respectively,

$$P_m = \frac{Q_m(s)}{\tau_m(s) - KN^{-1}Q_d(s)} = (\frac{1}{J_m s^2 + B_m s}) \tag{4}$$

where P_m is the motor side transfer function with the input-output relation of difference of the motor torque and the output torque to the motor position. J_m and B_m is the inertia viscous friction of the motor side, respectively.

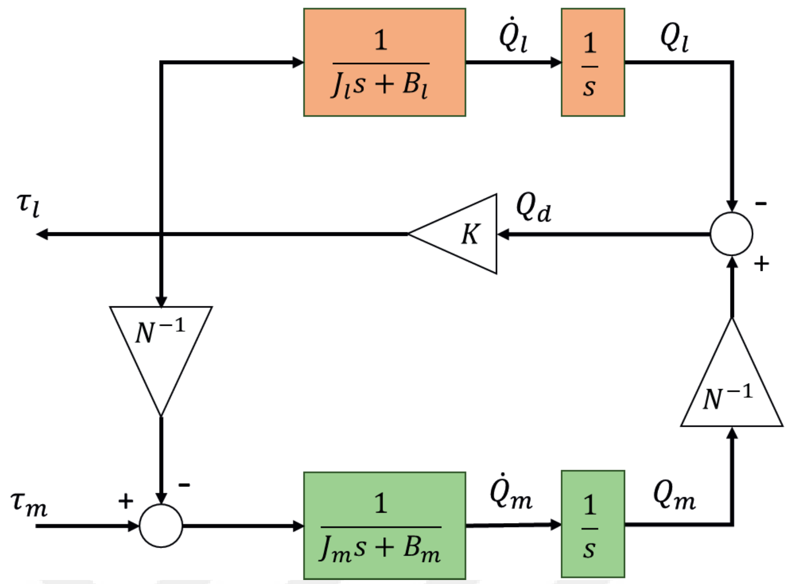

Figure 18: Block diagram of the SEA model

$$P_l = \frac{Q_l(s)}{\tau_l(s)} = (\frac{1}{J_l s^2 + B_l s}) \tag{5}$$

P_l is the transfer function of the link side with the input-output relation of output torque to the link position.

One can obtain the transfer function where the input is the motor torque τ_m and the output is the deflection of the spring Q_d. By utilizing eq. 4 and 5,

$$Q_d(s) = \frac{P_m N^{-1} \tau_m}{1 + K N^{-2} P_m + K P_l} \tag{6}$$

3.1.2 System Identification for Motor Side

We can calculate the system parameters such as inertia and viscous friction of the motor side using the CAD design. However, data from the CAD cannot be accurate due to the manufacturing phase. In order to increase the performance of the controllers, these parameters can be determined by applying system identification onto the motor side of the SEA.

First, stiction compensation should be applied to the actuator in order to reduce

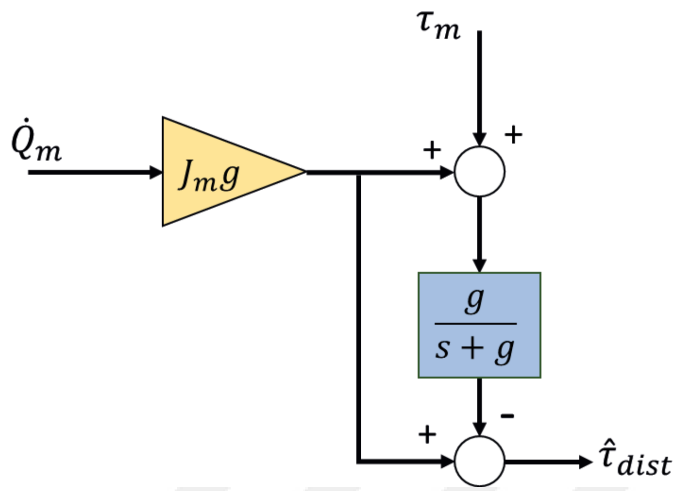

Figure 19: Block diagram of the disturbance observer model

the friction component. Ramp current is applied to the actuator and motor position and velocity are measured using the encoder. Disturbance of the internal system is also required, therefore, we applied a DOB to the motor side. The DOB estimates the disturbances acting on a system by using the nominal values of the plant [46]. The values for the actuator is gathered from the CAD data and the nominal model is formed. In Fig. 19, block diagram of the disturbance observer is can be seen where g is the frequency of the DOB.

The friction and the stiction curves of the actuator can be obtained by plotting the disturbance with respect to the velocity. In Fig. 20, the uncompensated curve can be seen. For the positive direction, $0.10831Nm$ torque required to compensate the stiction while for the negative side, $0.09482Nm$ was enough.

After the stiction compensation is applied, MATLAB System Identification Toolbox was used to identify the system parameters of SEA.

3.1.3 Torque Control

SEA is a compliant actuator as stated above, thus, it has superior properties with respect to stiff actuators. On the other hand, due to the complexity in the high-order

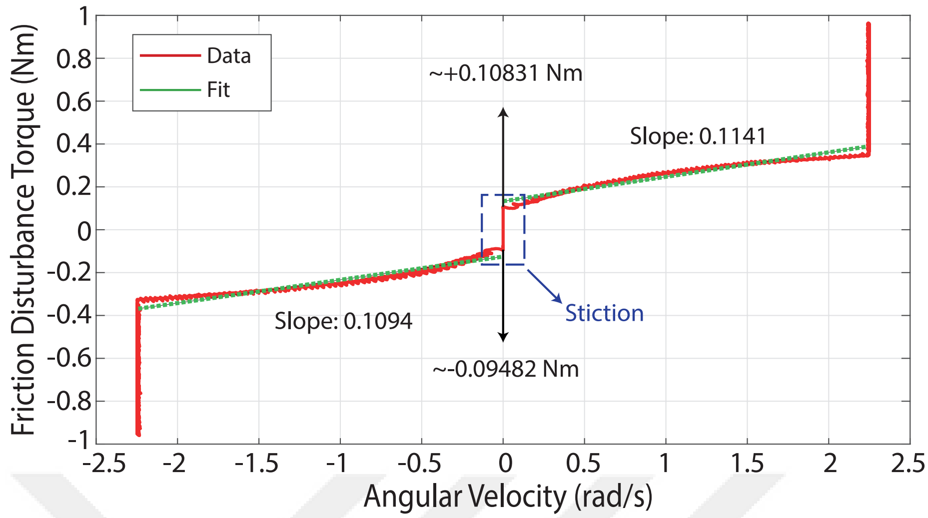

Figure 20: Uncompensated motor frictional torque curve

dynamical model of SEA, friction between the components, backlash and the nonlinearity of the actuator model; it requires advanced controllers rather than traditional methods.

There are various available controller methods applied to SEAs in the literature. Pratt et al. initially implemented a PID controller for torque control. However, the controller's performance was unsatisfactory; therefore, they added a FF to satisfy the non-modeled dynamical effects [47]. In [48], they implemented a PD controller with feed-forward for the elastic joints. Nonetheless, the system's overall performance may be reduced because of the non-linear disturbances acting on the system; thus, these controllers are deemed insufficient for robust tracking. In [49], Wyeth suggested a cascaded controller where a velocity controller is applied in the inner loop, and a torque controller is implemented in the outer loop. In this way, minimizing the non-linearities like stiction is aimed. Later on, Heike et al. studied the cascaded controller and aimed to develop the stability of the method [50]. In [51], Ugurlu et al. tested different controllers and created a benchmarking for torque control strategies. Following their steps, a torque controller is implemented to our SEAs.

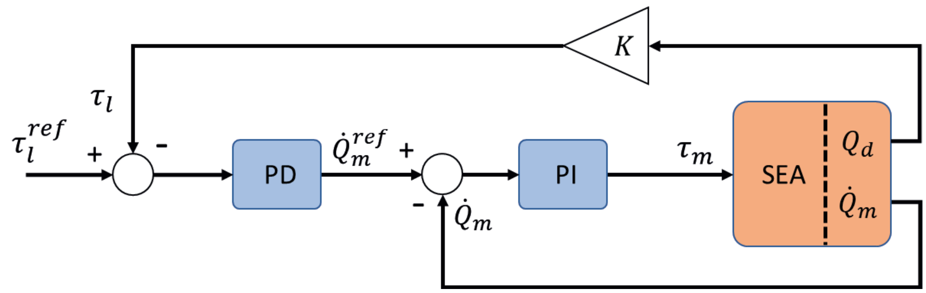

Figure 21: Block diagram of cascaded control with torque outer-loop and velocity inner-loop

Cascaded PID Controller with DOB

Cascaded PID controller is implemented for the torque control of the SEA. Cascaded controller refers to multiple control loops where outer one generates the input for the inner loop. It is claimed that, if the inner-loop has high-frequency, the outer-loop force control indicates better tracking results [50]. The cascaded controller used in the system is shown in Fig. 21. In this controller, the outer-loop feeds the difference between reference link torque and the output torque to the PD controller. The output of the PD controller develops the reference motor velocity and it is fed to the PI controller to achieve the motor torque. There was no filter applied for the actual motor velocity since the encoder gives a result that is not noisy.

However, there is approximately 10% backlash due to the encoder reading of the torsional spring and this makes it difficult to create a robust torque control. To overcome this issue, a disturbance observer is applied to the SEA. With this way, deflection is measured and fed back to the system directly [52].

After adding the disturbance observer, backlash in the system has been largely reduced. In this way, the series elastic actuator can work sensitively against external forces. In order to test the torque reading performance of the system, actuator was operated with zero torque input and external force was applied. When the external force is applied to the actuator in the positive direction, current is supplied to the motor in the opposite way. Thus, the output link of the actuator can rotate in the

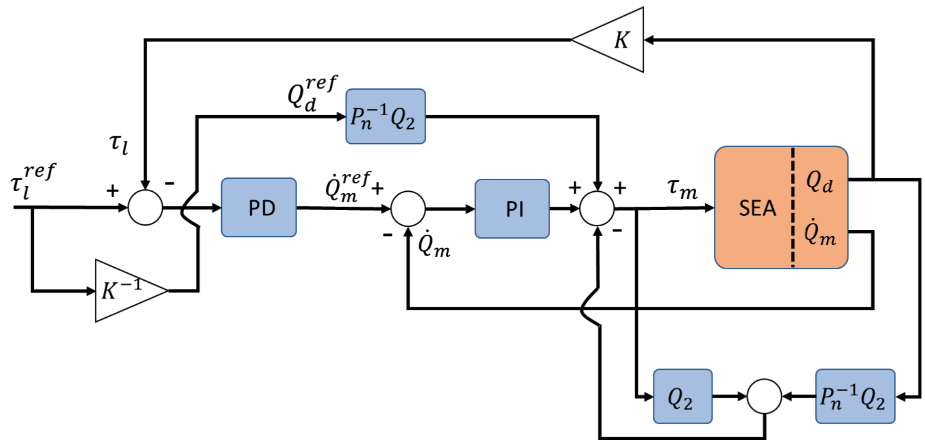

Figure 22: Block diagram of cascaded control with disturbance observer added

same direction as the external force while without applying any resistance. Result of the zero torque control is shown in Fig. 23.

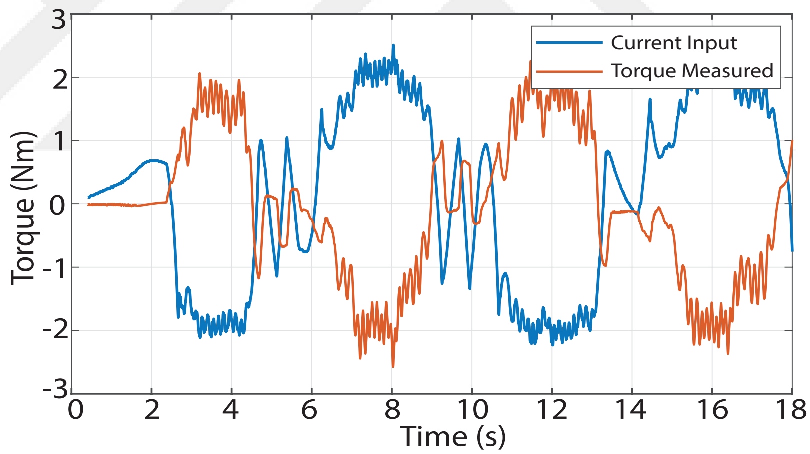

Figure 23: Zero Torque Control performance of the cascaded PID controller with FF + DOB

3.1.4 Position Control

In order for the exoskeleton to perform actions such as walking and sitting-standing, its joints must be able to track given reference angles. For this reason, a position controller is applied to the series elastic actuator. Cascaded PID with disturbance observer is used as inner system and one more loop is added on top of it. Reference joint position is given as input and reference joint torque is obtained as output

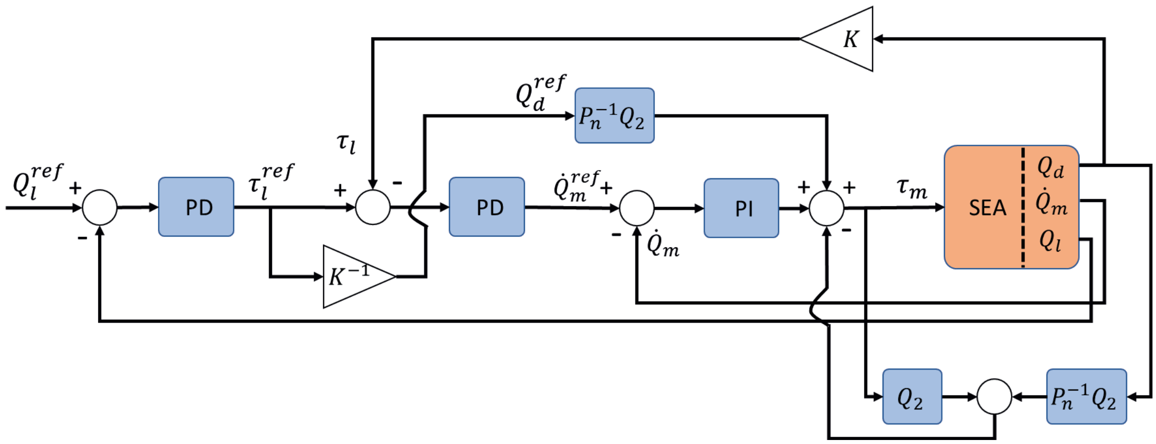

Figure 24: Block diagram of cascaded control with added position controller

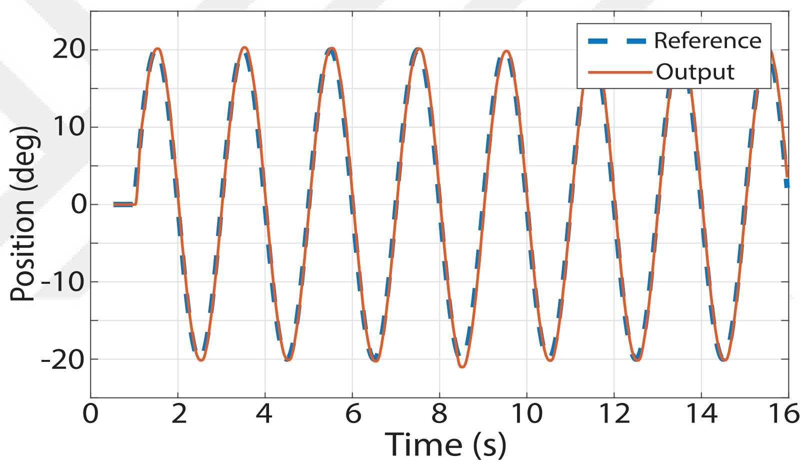

Figure 25: Position control with ±20 deg reference input at 0.5 Hz frequency

from the implemented PD controller. You can see the block diagram of the position controller in Fig. 24.

In order to test the performance of the designed position controller for different references, sine waves at various speeds were given and the tracking performances were obtained. Performance of the position controller at 0.5 Hz frequency with ±20 degree angle reference is given in Fig. 25. Performance of the controller at frequency of 2 Hz and joint position reference of ±5 degrees is also given in Fig. 26.

The average walking gait frequency of healthy person ranges from 1.4 Hz to 2.3 Hz [53]. Since the purpose of the exoskeleton is rehabilitation, it is expected to walk

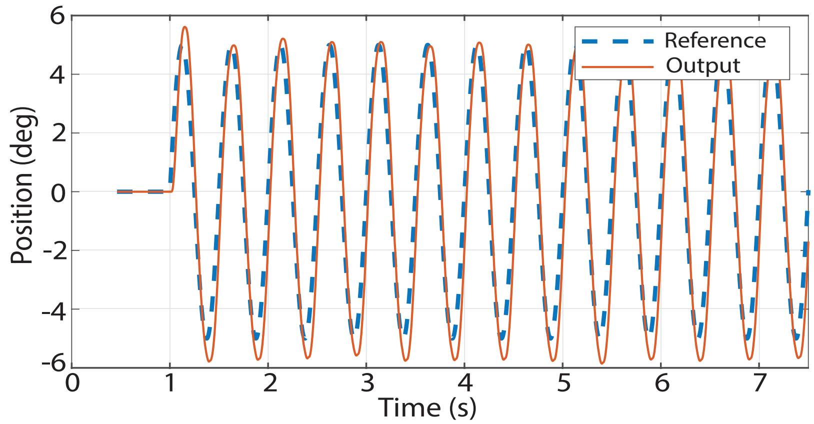

Figure 26: Position control with ±5 deg reference input at 2 Hz frequency

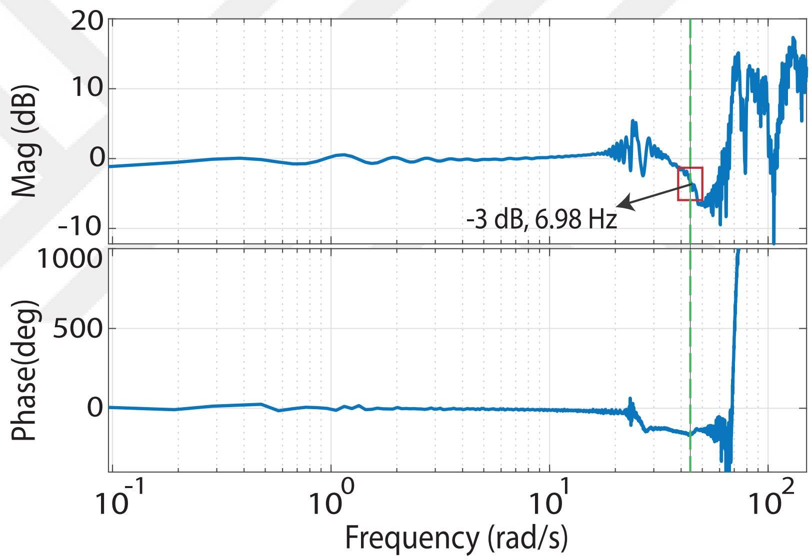

Figure 27: Bode plot of the cascaded PID controller with FF + DOB and position controller

a little slower than or similar to a healthy human walking speed. As a result of the experiments done on position controller, it is shown that the tracking performance is satisfying at 2 Hz.

In order to investigate the stability of the controller against varying frequencies, bode diagram should be plotted. Bode plot is a graph where magnitude (in dB) is compared against frequency. To create a bode diagram, chirp signal is given as input to the actuator with the frequency range of 0.1 Hz to 8 Hz. Tracking performance is gathered from the experiments and bode diagram is plotted as given in Fig. 27.

We can detect the bandwidth of the system where controller acts stable by checking the plot where magnitude passes -3 dB first time. According to the bode diagram, controller exhibited up-to 6.98 Hz control bandwidth. Thus, a healthy human's walking gait frequency can be achieved using suggested series elastic actuators.

3.2 Locomotion Method

3.2.1 Simulation Structure

In order to implement a desired motion to the exoskeleton, different locomotion methods should be created. Since walking and sitting/standing or squat motions are the most frequent motions that happens in a day, they are selected as targets. Sitting/standing and squat motions have very simple trajectories similar to sine wave however walking is not a simple task to achieve. Before trying them on the exoskeleton, algorithms should be verified on a simulator. MSC ADAMS's dynamic contact solving quality found to be poor, therefore a different dynamics simulator is selected for simulations. RaiSim v1.1.5 is used during the locomotion algorithm development. RaiSim is a multi-body physics engine for robotics and AI applications where contact dynamics problems are solved with an efficient bisection method [54]. Moreover, simulator is working with C++ language so that, when the algorithms approved on simulation, they can be directly transferred to the exoskeleton.

In the model, robot is constrained along the sagittal plane to be able to make the robot walk. Since there are no A/A joint on the exoskeleton, it cannot sway its COM. Without these constraints or without implementing crutches in the simulation, when the robot tries to raise a leg, it will fall sideways. Since the aim is testing locomotion algorithms, we can constraint the robot rather than implementing complex crutch mechanisms.

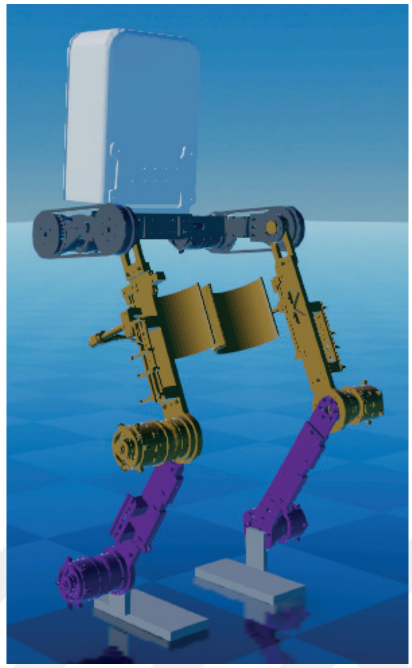

Figure 28: Exoskeleton model created in RaiSim

3.2.2 Trajectory Planning

Exoskeleton is a biped robot which has rectangular shaped foots. Walking can be achieved by moving the legs one by one in the same direction. Thus, we can generate a pattern which has three phases in general. Walking phase can be extended as long as it starts and ends with a double support phase. Transfer phases are important to move the foot a half step forward to start and end the walking.

- Transfer phase for starting movement (half step)
- Walking phase:
  - Double support phase
  - Single support phase
  - Double support phase
  - Single support phase
- Double + Transfer phase for finishing movement (half step)

In order to create this walking pattern, different methods are available in the literature. One of them is ZMP method which makes it possible to generate a trajectory for the COM while maintaining dynamic balance. ZMP-based pattern generation involves moving the COM in a manner that keeps the ZMP within the support polygon [55, 56, 57]. There are many studies on legged robotics that use ZMP to enable dynamically balanced COM trajectory [58, 59]. In order to create a dynamically balanced walking, ZMP-based trajectory generation is utilized.

ZMP is the point on the ground where moments on the horizontal plane acting on the robot's foot are zero. For ZMP concept to work, there should be no slipping between the ground and the contact surface. Dynamic balance can be achieved if the ZMP is inside the support polygon. Equations to generate ZMP and the algorithms can be seen in [56]. Since the exoskeleton can only move in the sagittal plane, there is no need to calculate the ZMP on y-axis.

3.2.3 Kinematics of the Robot

Exoskeleton has three active joints along hip F/E axis, knee F/E axis and Ankle DP/F axis, respectively. In order to compute corresponding joint angles for desired trajectory, inverse kinematics of the robot is utilized. Since exoskeleton is an under-actuated robot, kinematic model is divided into two parts; single leg and floating base kinematics. Due to its joint capabilities, exoskeleton cannot move laterally without any external assistance, i.e, crutches. Therefore, similar to the Raisim model where exoskeleton is constrained in the sagittal plane, uncontrollable freedoms of floating base are neglected. Kinematics scheme of the robot can be seen in Fig. 29.

3.2.4 Computed Torque Control - Lagrangian Based Dynamics

In order to calculate required joint torques for given trajectories, Lagrangian dynamics of the robot is utilized. Robot's dynamic system is solved in MATLAB and required matrices are gathered in order to calculate joint torques. Mass, centripetal

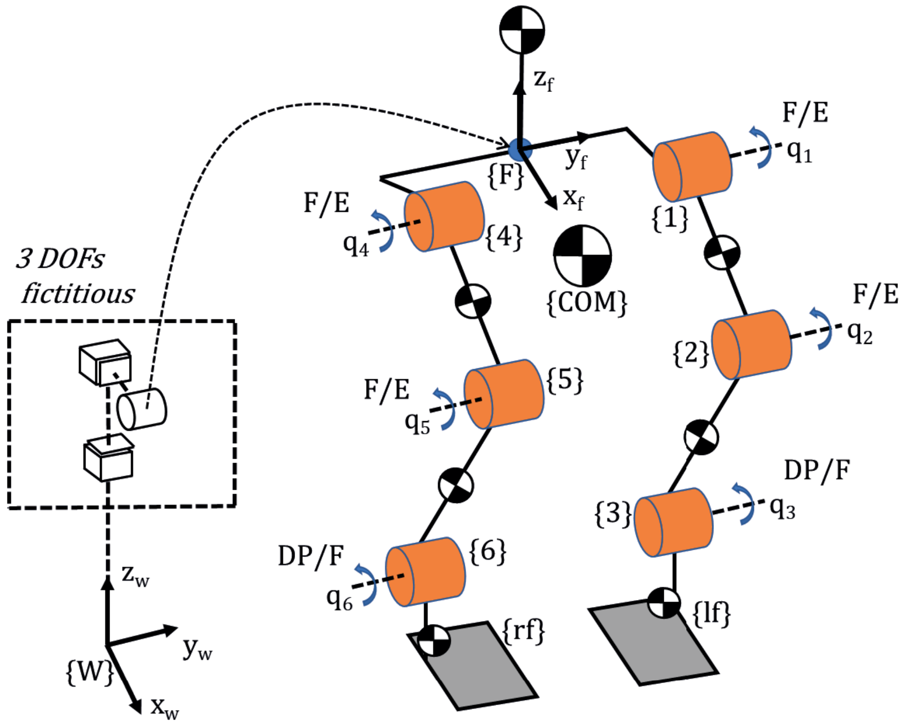

Figure 29: Kinematics diagram of the lower body exoskeleton

and Coriolis, gravitational and Jacobian matrices of the exoskeleton are utilized in a function to compute required joint torques. Equation of Lagrangian based inverse dynamics to calculate joint torques for given joint trajectories is as follows:

$$\tau = M(q)\ddot{q}_{ref} + C(q, \dot{q}) + G(q) + J^{\intercal} F_{ref} \quad (7)$$

In 7, $M(q)$ represents mass matrix, $C(q, \dot{q})$ is centripetal and Coriolis forces, $G(q)$ is gravitational forces, J is the Jacobian matrix of exoskeleton leg and F is the reference external forces which will act on the foot. Moreover, q, $\dot{q}$ and $\ddot{q}_{ref}$ are joint angles, joint velocities and reference joint accelerations, respectively. Using this equation with given matrices, required torques for each joint can be calculated.

3.2.5 Controller Strategy

A basic control diagram is shown in Fig. 30. Starting command comes from the main PC and ZMP based trajectory algorithm is used to define desired foot positions. To

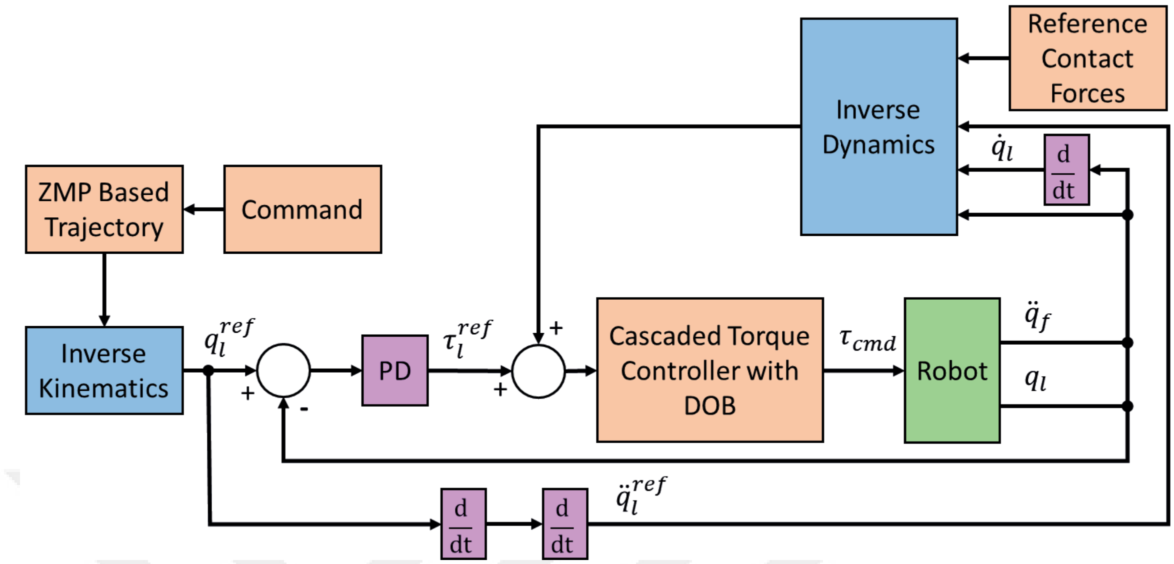

Figure 30: Basic control diagram of the lower body exoskeleton

implement these positions to the actuators, inverse kinematics is utilized by calculating joint angles for desired foot positions. PD position controller is implemented using given joint trajectories to determine required joint torques. Previously mentioned cascaded torque controller with DOB creates the torque command for motor drivers. Moreover, inverse dynamics of the system is implement using Lagrangian method so that robot's dynamics are modeled. Reference foot forces are generated as distribution of the total weight to the contact foots. With the implementation of inverse dynamics, PD gains of the position controller can be reduced.

CHAPTER IV

SIMULATION AND EXPERIMENTAL RESULTS

The exoskeleton design is subjected to simulations and experiments in order to validate its functionality and ascertain its potential for future rehabilitation applications. These assessments confirm the capability of the robot to perform walking tasks and provide evidence supporting its potential usefulness in rehabilitation contexts.

4.1 Walking Simulation

Prior to implementing algorithms on the robot, they are verified in the simulation environment. The simulation commences with the robot positioned with bent joints, prepared for walking. ZMP based walking trajectory is employed, with a forward velocity of $0.2m/s$. Since robot is constrained in the sagittal plane, the risk of lateral falls during walking is eliminated. Generated COM and feet trajectories can be seen in Fig. 31. Moreover, it is crucial to ensure dynamic balance by maintaining the ZMP locations within the boundaries of the support polygon during walking, as mentioned previously. Consequently, the ZMP response is carefully monitored, as depicted in Fig. 32 dynamic balance is ensured. Notably, as the simulation does not allow for movement along the y-axis, the plot only represents the x-axis ZMP.

The tracking performance of the joints is assessed both with and without the implementation of CTC. The joint tracking errors are compared specifically for the knee joint, as illustrated in Fig. 33. Each joint's tracking performances with CTC implemented are shown in Fig. 34-39. Furthermore, the RMS error for each joint is provided in Table 6, comparing the results between the two cases.

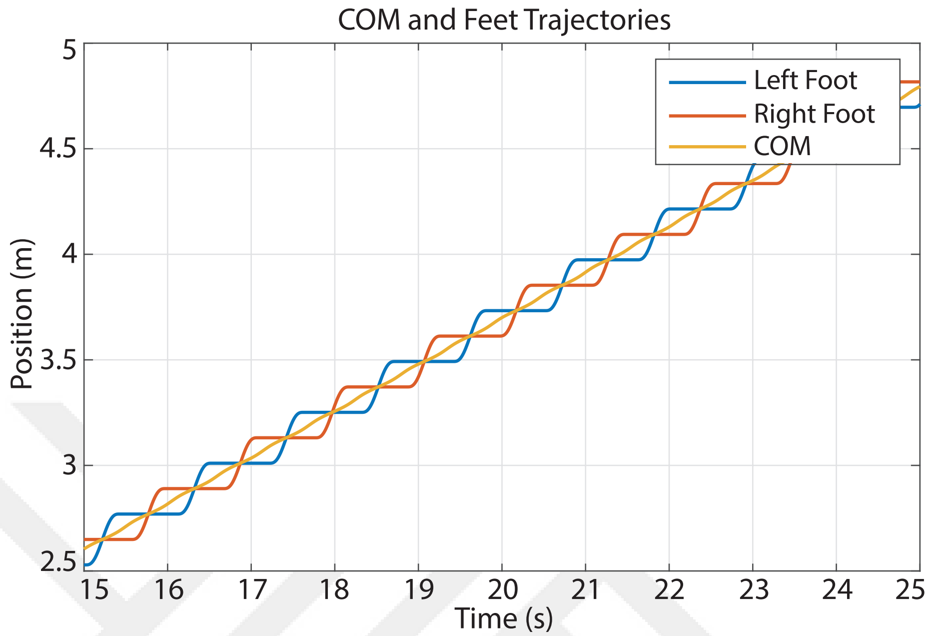

Figure 31: COM and feet trajectories generated from the algorithm

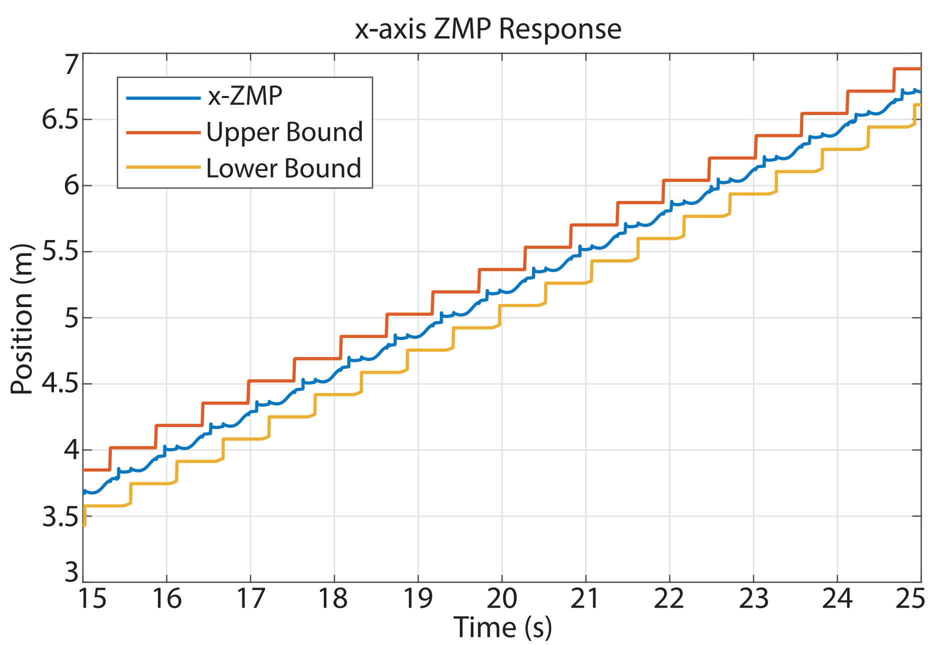

Figure 32: ZMP response of the exoskeleton along x-axis

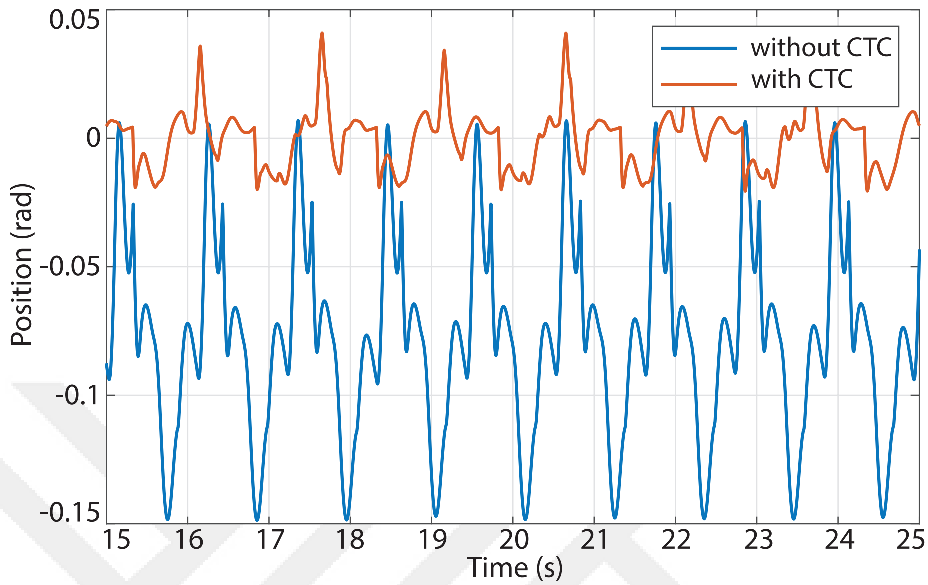

Figure 33: Joint tracking errors with and without CTC implemented in the simulation

Table 6: Joint tracking RMS errors while robot is walking in the simulation

Joint	Left Leg Joints RMSE (deg)	Right Leg Joints RMSE (deg)
	Without CTC	
Hip	2.6808	2.6810
Knee	4.8998	4.8788
Ankle	1.2119	1.2047
	With CTC	
Hip	0.8649	0.8642
Knee	0.6521	0.6545
Ankle	0.7112	0.7141
% Reduction in Error		
Hip	67.7	67.7
Knee	86.6	86.6
Ankle	41.3	41.3

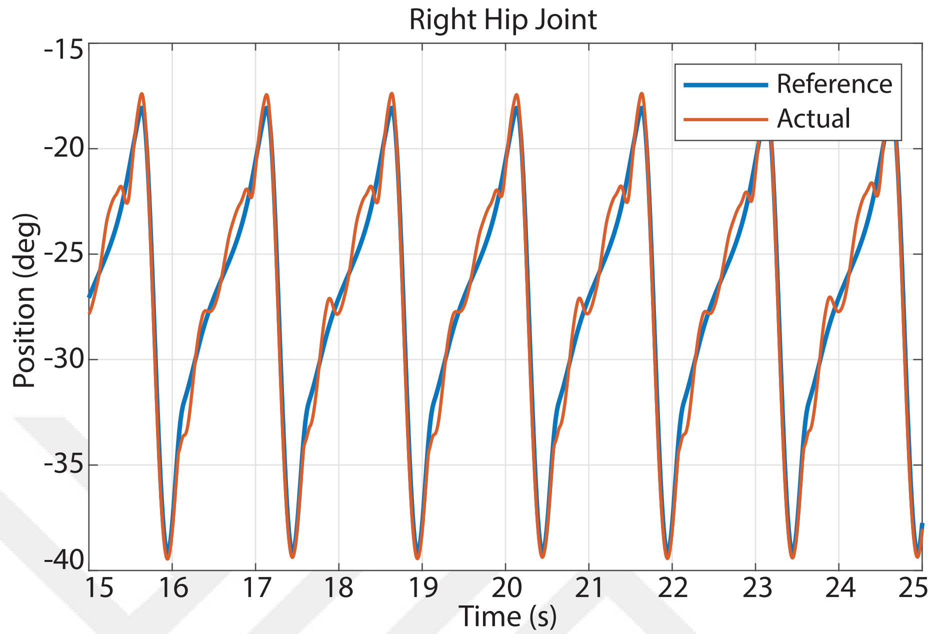

Figure 34: Right hip joint tracking with CTC implemented during walking in simulation

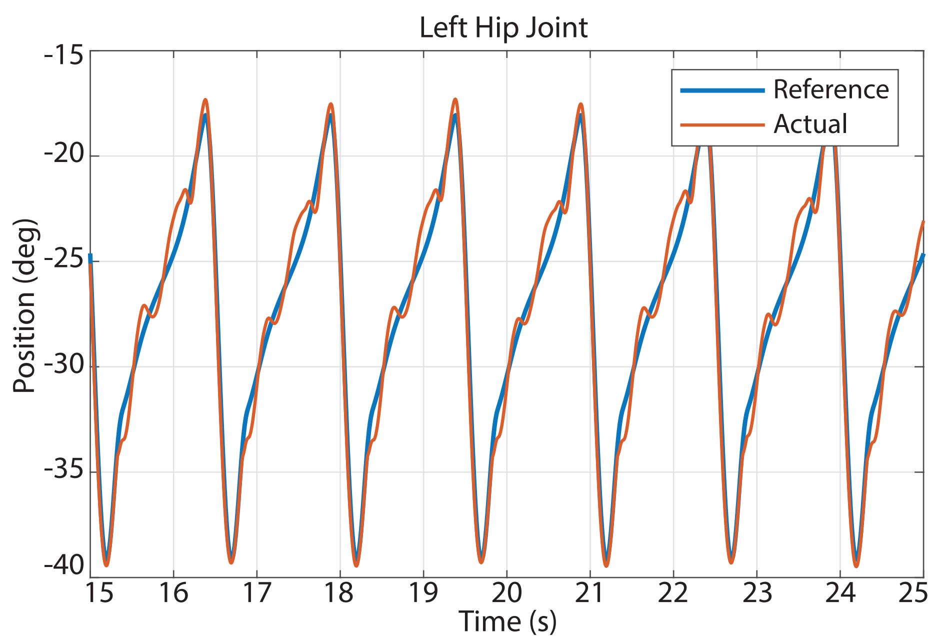

Figure 35: Left hip joint tracking with CTC implemented during walking in simulation

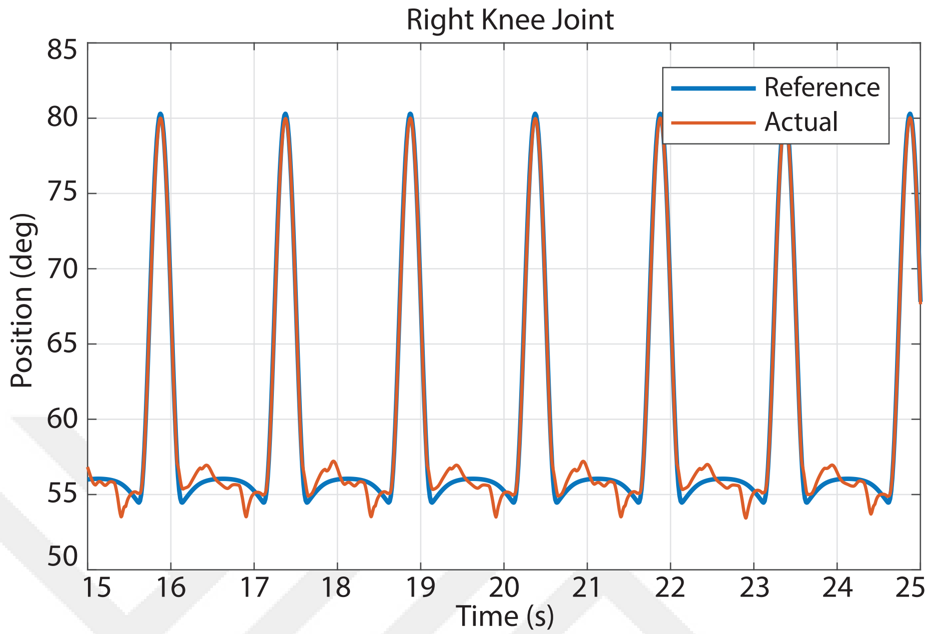

Figure 36: Right knee joint tracking with CTC implemented during walking in simulation

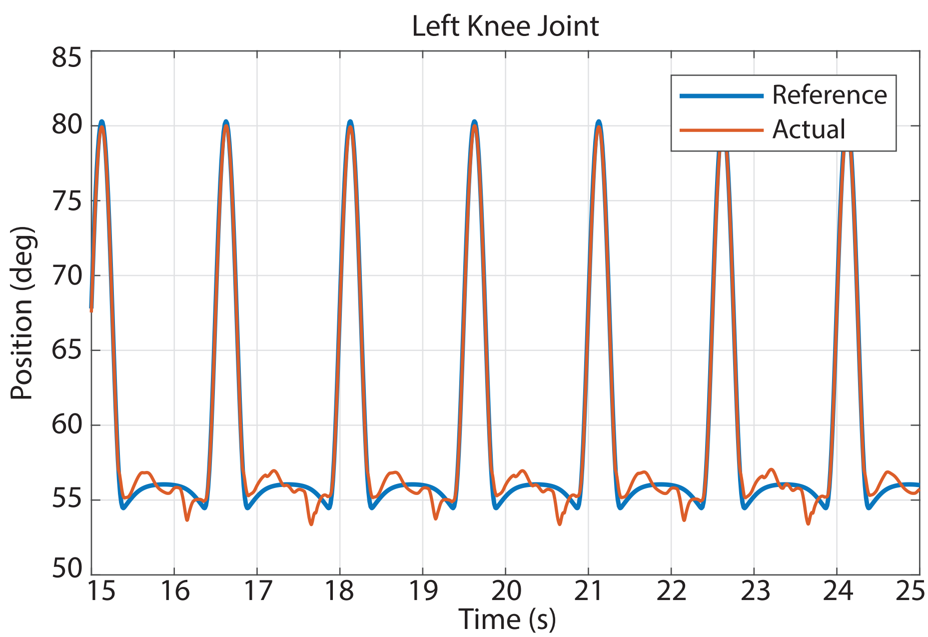

Figure 37: Left knee joint tracking with CTC implemented during walking in simulation

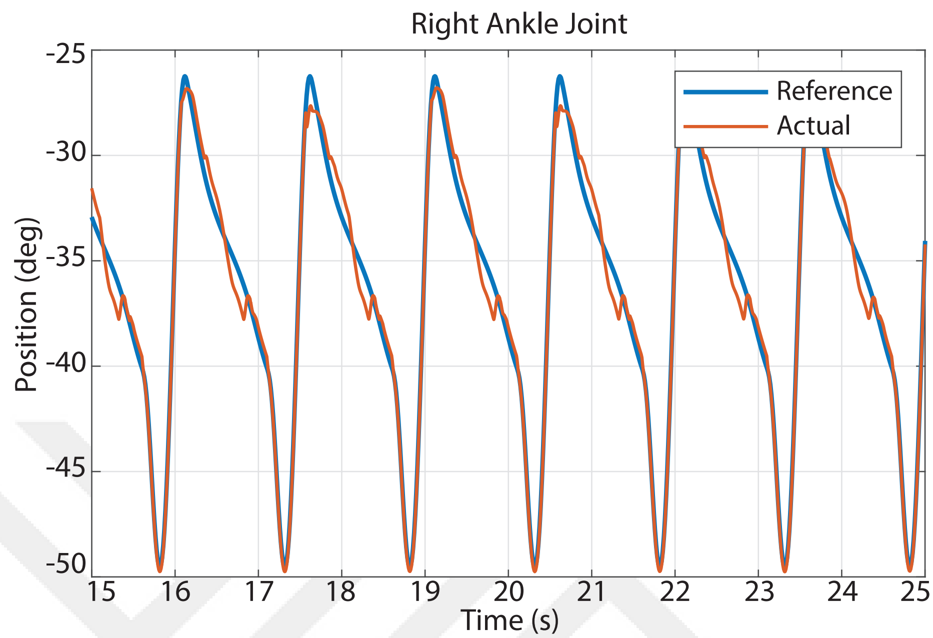

Figure 38: Right ankle joint tracking with CTC implemented during walking in simulation

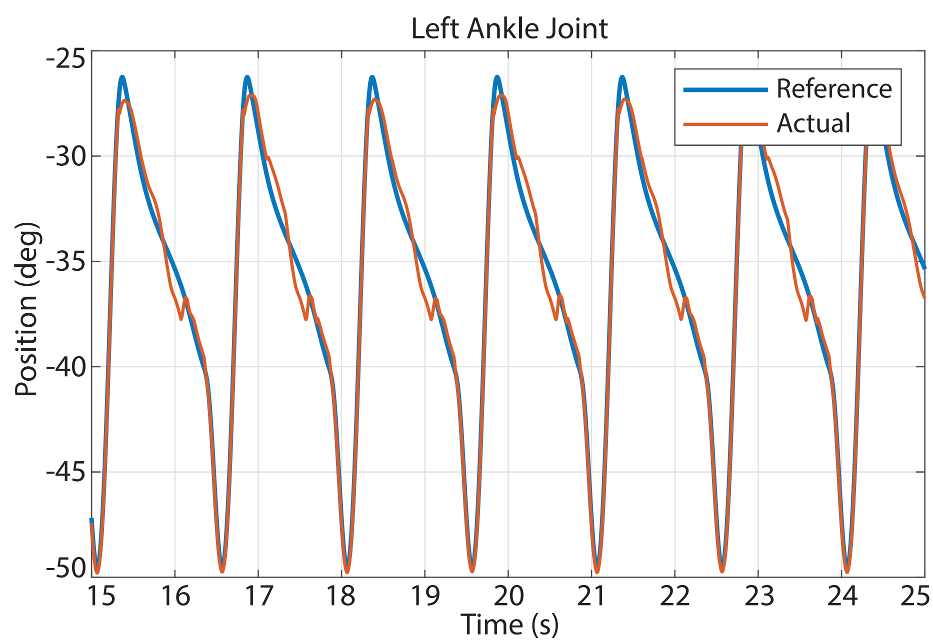

Figure 39: Left ankle joint tracking with CTC implemented during walking in simulation

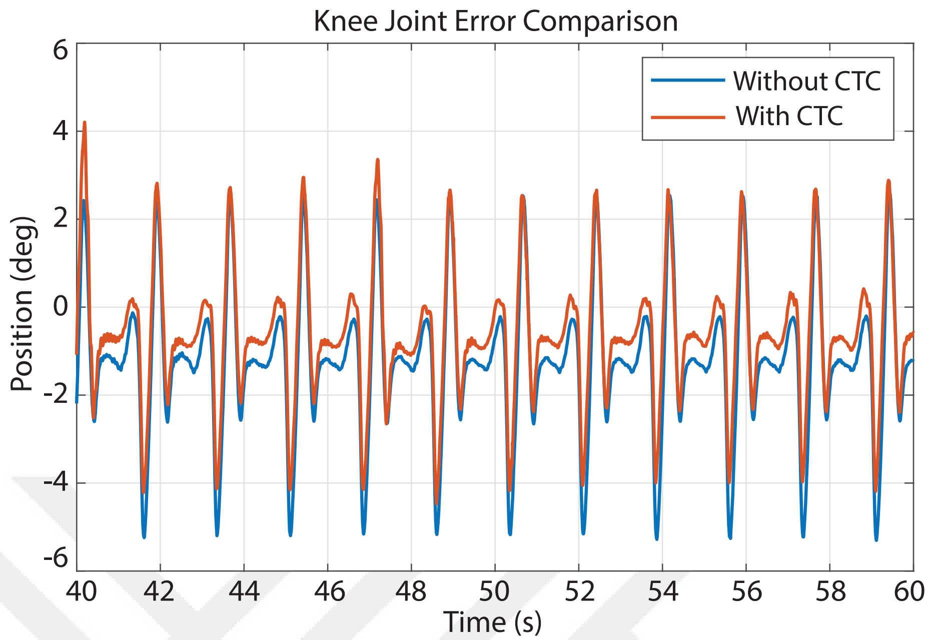

Figure 40: Joint tracking errors with and without CTC implemented while robot is hanging

4.2 Walking Experiment

The walking algorithms are executed on the lower body exoskeleton. Initially, a step-by-step assessment is conducted on each joint to identify any potential issues. Subsequently, the walking algorithm is evaluated with the application of high PD gains and CTC. To ensure safety, initial experiments are performed with the exoskeleton in a suspended state.

Walking While Hanged - 0.2 m/s Forward Velocity

Before placing the robot on the ground, the performance of controllers and locomotion strategies was examined while the robot is tethered. the robot was assigned a forward velocity of 0.2 m/s, and walking trajectory was generated utilizing ZMP-based trajectory planner. Firstly, the tracking performance of each joint was evaluated both with and without the implementation of CTC, as depicted in the Fig. 40 Furthermore, Table 7 presents the RMS error for each joint. The individual tracking performances of each joint, with CTC implemented, are illustrated in Fig. 41-46.

Table 7: Joint tracking RMS errors while robot is hanging

Joint	Left Leg Joints RMSE (deg)	Right Leg Joints RMSE (deg)
	Without CTC	
Hip	1.9462	1.6768
Knee	1.4934	2.0562
Ankle	1.1268	0.8067
	With CTC	
Hip	1.3510	0.8543
Knee	0.9944	1.0854
Ankle	0.9816	0.6843
% Reduction in Error		
Hip	30.5	49
Knee	33.4	47.2
Ankle	12.8	15.1

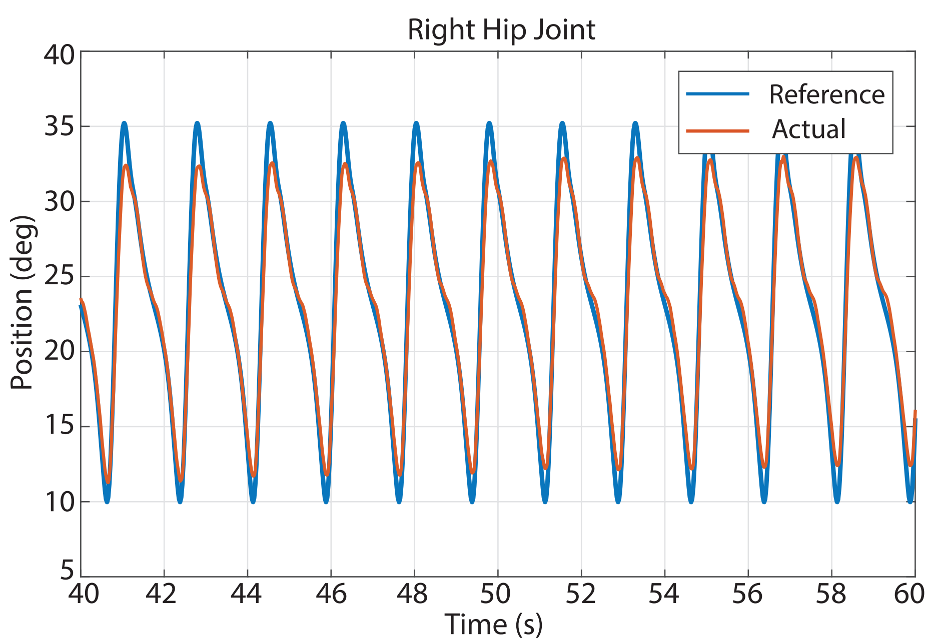

Figure 41: Right hip joint tracking with CTC implemented during walking while hanging

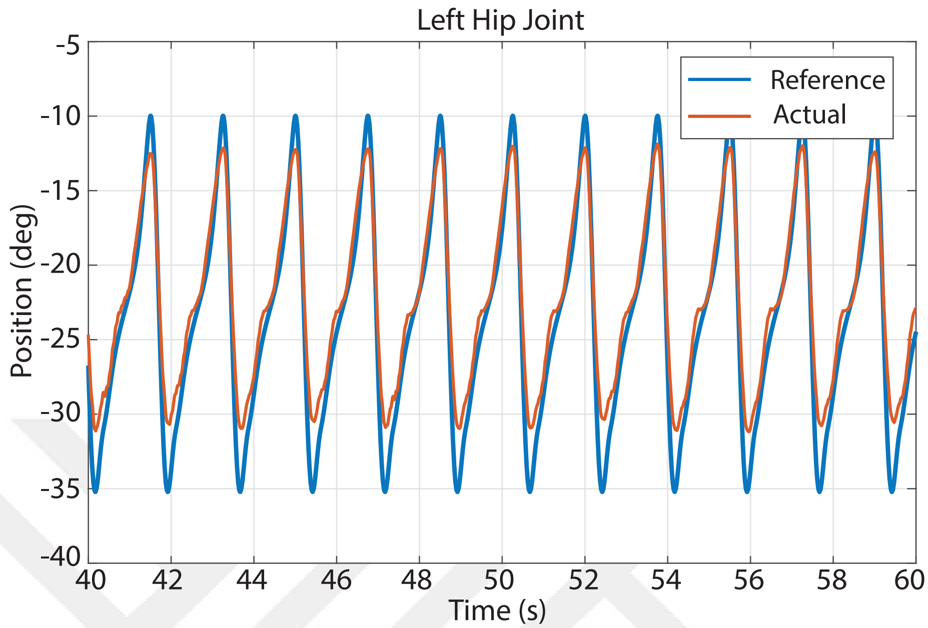

Figure 42: Left hip joint tracking with CTC implemented during walking while hanging

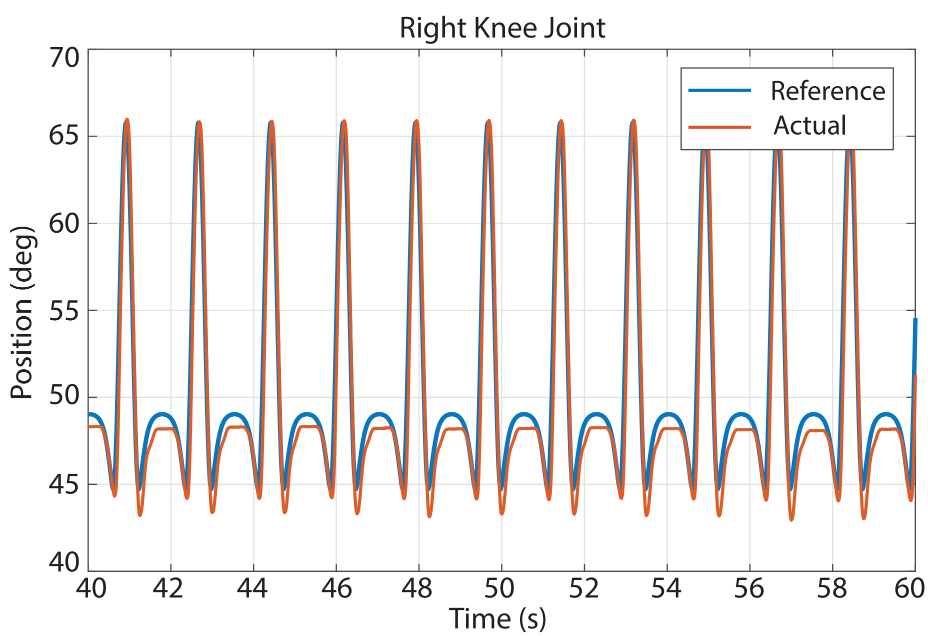

Figure 43: Right knee joint tracking with CTC implemented during walking while hanging

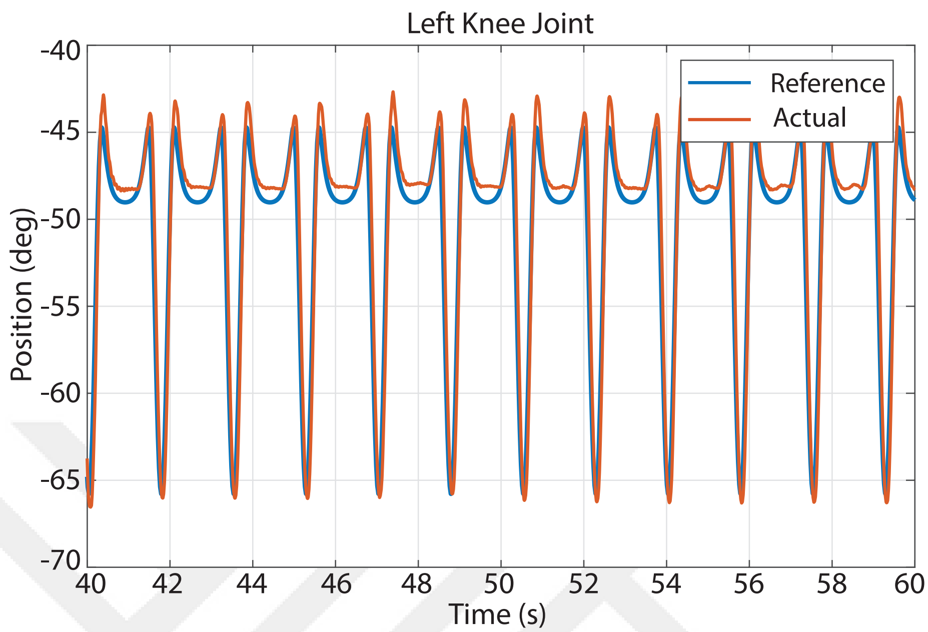

Figure 44: Left knee joint tracking with CTC implemented during walking while hanging

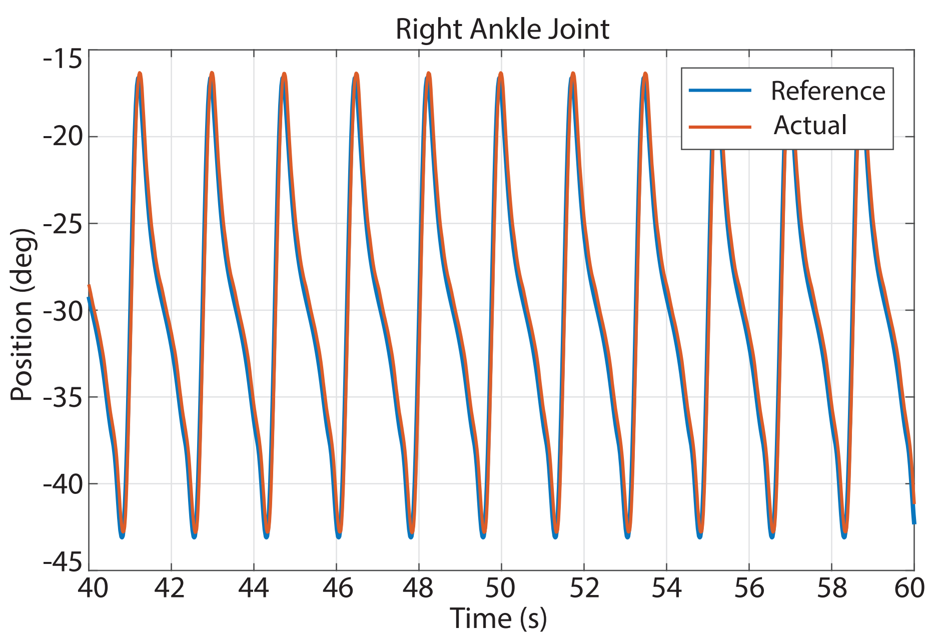

Figure 45: Right ankle joint tracking with CTC implemented during walking while hanging

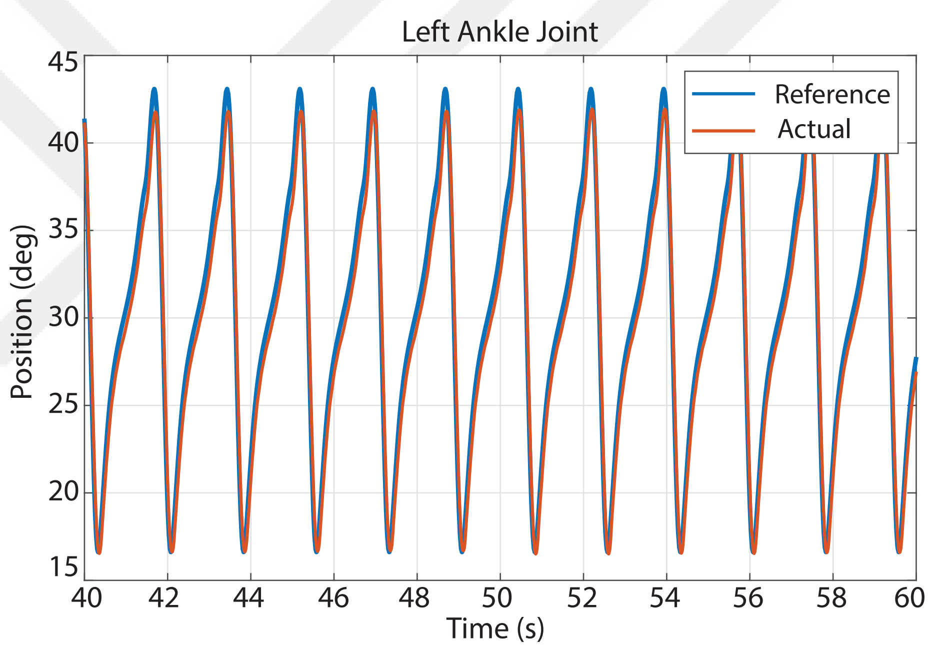

Figure 46: Left ankle joint tracking with CTC implemented during walking while hanging

CHAPTER V

CONCLUSIONS

This thesis proposes a comprehensive framework encompassing the design, development, and force control implementation of a wearable lower-extremity exoskeleton capable of achieving complete balance along the sagittal plane.

To determine the optimal placements of the hip, knee, and ankle actuators, an iterative study was conducted. The knee and ankle actuators were directly attached to the joints, while the hip actuator was positioned at the back waist area to improve wearability. A coupled human-exoskeleton model was constructed, and two simulation scenarios were considered: stand-to-sit and dynamic walking motion. Through these simulations, mechanical loading and actuator torques were obtained. Evaluating the joint torques derived from the simulations, two different SEA units were identified for actuating the joints. Additionally, a topology optimization approach coupled with stress analysis was employed on each link, utilizing the maximum load experienced by the joints, with the aim of reducing the weight of the exoskeleton. The simulations resulted in the successful achievement of sitting motion and validation of dynamic balance, since the ZMP response was maintained within the support polygon. The proposed methodology demonstrated the convenience of designing exoskeletons for diverse tasks, considering essential evaluation indicators such as joint range, torque controllability, weight reduction, and wearability.

Upon validating the exoskeleton design, each component was manufactured and assembled. Nvidia Jetson AGX Xavier was chosen as the primary controller for the robot. The communication system of the exoskeleton relied entirely on the EtherCAT system, where Xavier served as the master while motor drivers, A/D shields, and other devices operated as slaves. High-resolution absolute rotary encoders were employed to accurately measure motor and link positions. To enable the integration of link encoders, a custom-made EtherCAT shield circuit was utilized. EsmaCAT's A/D shields were conducted in implementing the sensorized shoe and the smart cloth into the robot. To minimize cable mass, certain electronic components were placed on the exoskeleton's legs, and EtherCAT communication was facilitated by connecting Ethernet cables in a chain-like configuration.

To identify system parameters, a DOB was applied to the motor side of the SEA. The friction and stiction curves of the actuator were obtained by plotting the disturbance torque against velocity. Due to the complex nature of the SEA, several advanced controllers were tested. Initially, a cascaded PID controller was implemented for SEA torque control; however, approximately 10% backlash caused by the encoder reading of the torsional spring posed challenges in achieving robust torque control. To overcome this issue, a disturbance observer was introduced to the SEA, resulting in a significant reduction in backlash. To validate the torque reading performance, the actuator was operated with zero torque input while external forces were applied. Additionally, a position controller was incorporated into the outer loop of the cascaded controller. Performance of the position controller was assessed by subjecting it to sine waves at various frequencies, and the tracking performances were evaluated. Furthermore, a bode diagram analysis was conducted to investigate the stability of the controller against varying frequencies, which revealed that the system remained stable within a bandwidth of up to 6.98 Hz.

In order to achieve the desired motion of the exoskeleton, locomotion methods were initially tested through simulations before being applied to the robot. To establish a walking pattern, ZMP method were employed. Trajectory planner successfully generated feasible COM and feet trajectories. Notably, the ZMP positions consistently stayed within the support polygon, resulting in dynamically balanced walking.

To enhance controller stability, the Lagrangian dynamics of the robot were utilized. Both in simulations and experiments, the robot demonstrated successful walking at a given trajectory with a forward velocity of 0.2 m/s.

In conclusion, this thesis has encompassed the design, development, and controller implementation of a wearable exoskeleton with a high power-to-weight ratio. The proposed design and methods underwent rigorous testing in simulation environments, and subsequent experiments were conducted on the exoskeleton constructed based on the proposed design. The findings affirm the successful construction of the wearable exoskeleton, demonstrating its capability to achieve dynamic balance and perform walking tasks.

APPENDIX A

EXOSKELETON WITH HUMAN SUBJECT

Figure 47: Exoskeleton with healthy male subject

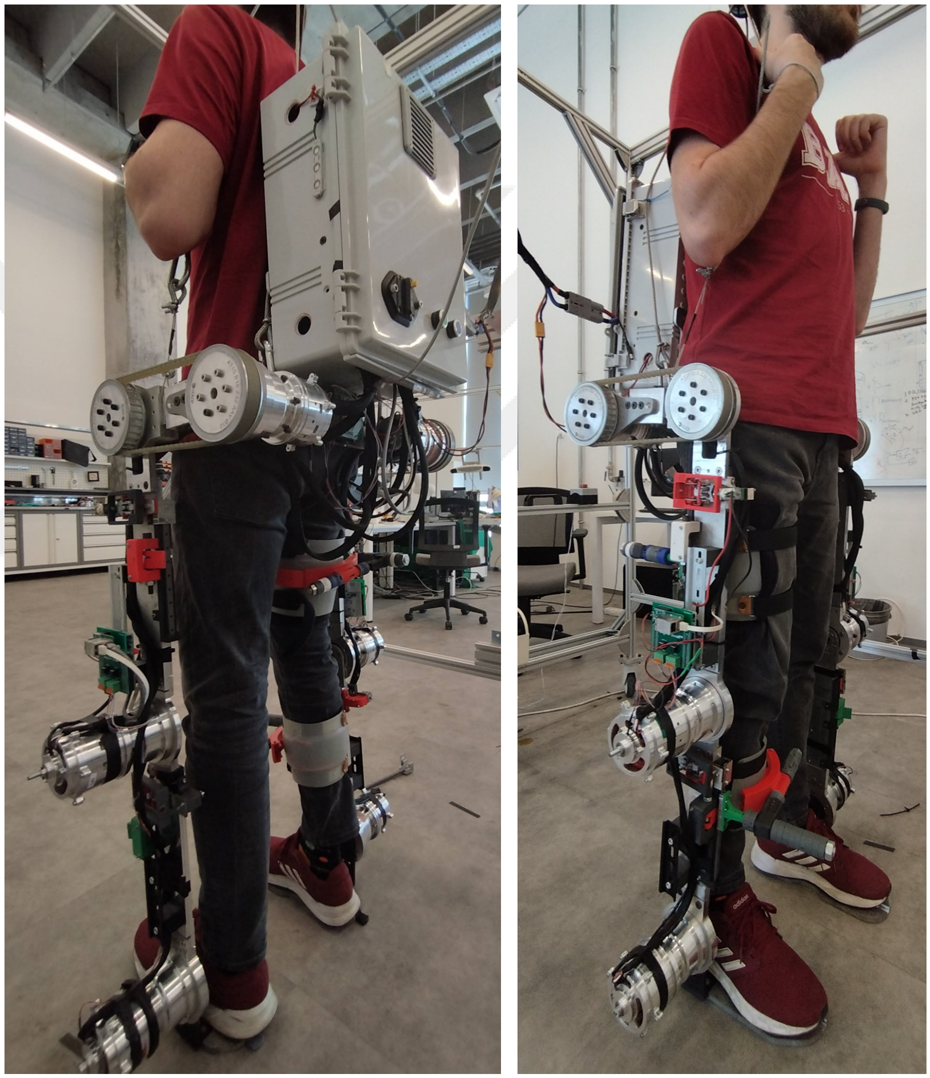

Figure 48: Exoskeleton with healthy male subject from back and side

REFERENCES

[1] O. M. Katalinic, L. A. Harvey, and R. D. Herbert, "Effectiveness of stretch for the treatment and prevention of contractures in people with neurological conditions: a systematic review," *Physical Therapy*, vol. 91, no. 1, pp. 11–24, 2011.

[2] D. U. Jette, N. K. Latham, R. J. Smout, J. Gassaway, M. D. Slavin, and S. D. Horn, "Physical therapy interventions for patients with stroke in inpatient rehabilitation facilities," *Physical Therapy*, vol. 85, no. 3, pp. 238–248, 2005.

[3] P. J. van der Wees, A. F. Lenssen, E. J. Hendriks, D. J. Stomp, J. Dekker, and R. A. de Bie, "Effectiveness of exercise therapy and manual mobilisation in acute ankle sprain and functional instability: a systematic review," *Australian Journal of Physiotherapy*, vol. 52, no. 1, pp. 27–37, 2006.

[4] M. Byrnes, J. Beilby, P. Ray, R. McLennan, J. Ker, and S. Schug, "Patient-focused goal planning process and outcome after spinal cord injury rehabilitation: quantitative and qualitative audit," *Clinical Rehabilitation*, vol. 26, no. 12, pp. 1141–1149, 2012.

[5] G. Hornby, D. Campbell, D. Zemon, and J. Kahn, "Clinical and quantitative evaluation of robotic-assisted treadmill walking to retrain ambulation after spinal cord injury," *Topics in Spinal Cord Injury Rehabilitation*, vol. 11, no. 2, pp. 1–17, 2005.

[6] G. Zeilig, H. Weingarden, M. Zwecker, I. Dudkiewicz, A. Bloch, and A. Esquenazi, "Safety and tolerance of the rewalk™ exoskeleton suit for ambulation by people with complete spinal cord injury: A pilot study," *The Journal of Spinal Cord Medicine*, vol. 35, no. 2, pp. 96–101, 2012.

[7] W. Lu, Y. Zheng, D. Yini, T. Meiling, X. Zhang, Y. Cheng, X. Zhang, and L. Xiao, "Effects of robot-assisted training on balance function in patients with stroke: A systematic review and meta-analysis," *Journal of Rehabilitation Medicine*, vol. 53, no. 4, 2021.

[8] A. Esquenazi, M. Talaty, A. Packel, and M. Saulino, "The rewalk powered exoskeleton to restore ambulatory function to individuals with thoracic-level motor-complete spinal cord injury," *American Journal of Physical Medicine & Rehabilitation*, vol. 91, no. 11, pp. 911–921, 2012.

[9] V. Lajeunesse, C. Vincent, F. Routhier, E. Careau, and F. Michaud, "Exoskeletons' design and usefulness evidence according to a systematic review of lower limb exoskeletons used for functional mobility by people with spinal cord injury,"

Disability and Rehabilitation: Assistive Technology, vol. 11, no. 7, pp. 535–547, 2016. PMID: 26340538.

[10] A. Rodríguez-Fernández, J. Lobo-Prat, and J. M. Font-Llagunes, "Systematic review on wearable lower-limb exoskeletons for gait training in neuromuscular impairments," *Journal of Neuroengineering and Rehabilitation*, vol. 18, no. 1, pp. 1–21, 2021.

[11] A. D. Gardner, J. Potgieter, and F. K. Noble, "A review of commercially available exoskeletons' capabilities," in *24th International Conference on Mechatronics and Machine Vision in Practice (M2VIP)*, pp. 1–5, 2017.

[12] A. Tsukahara, Y. Hasegawa, K. Eguchi, and Y. Sankai, "Restoration of gait for spinal cord injury patients using HAL with intention estimator for preferable swing speed," *IEEE Transactions on Neural Systems and Rehabilitation Engineering*, vol. 23, pp. 308–318, Mar. 2015.

[13] A. Kozlowski, T. Bryce, and M. Dijkers, "Time and effort required by persons with spinal cord injury to learn to use a powered exoskeleton for assisted walking," *Topics in Spinal Cord Injury Rehabilitation*, vol. 21, pp. 110–121, Mar. 2015.

[14] G. Hardin, R. Benya, and J. Kasanin, "Methods and apparatus for supporting content distribution," May 7 2013. US Patent 8,438,603.

[15] A. J. Young and D. P. Ferris, "State of the art and future directions for lower limb robotic exoskeletons," *IEEE Transactions on Neural Systems and Rehabilitation Engineering*, vol. 25, pp. 171–182, Feb. 2017.

[16] B. Ugurlu, H. Oshima, E. Sariyildiz, T. Narikiyo, and J. Babic, "Active compliance control reduces upper body effort in exoskeleton-supported walking," *IEEE Transactions on Human-Machine Systems*, vol. 50, pp. 144–153, Apr. 2020.

[17] C. Mummolo, W. Z. Peng, S. Agarwal, R. Griffin, P. D. Neuhaus, and J. H. Kim, "Stability of mina v2 for robot-assisted balance and locomotion," *Frontiers in Neurorobotics*, vol. 12, Oct. 2018.

[18] Y. Lee, Y.-J. Kim, J. Lee, M. Lee, B. Choi, J. Kim, Y. J. Park, and J. Choi, "Biomechanical design of a novel flexible exoskeleton for lower extremities," *IEEE/ASME Transactions on Mechatronics*, vol. 22, pp. 2058–2069, Oct. 2017.

[19] F. Sado, H. J. Yap, R. A. R. Ghazilla, and N. Ahmad, "Design and control of a wearable lower-body exoskeleton for squatting and walking assistance in manual handling works," *Mechatronics*, vol. 63, p. 102272, Nov. 2019.

[20] V. Lajeunesse, C. Vincent, F. Routhier, E. Careau, and F. Michaud, "Exoskeletons' design and usefulness evidence according to a systematic review of lower limb exoskeletons used for functional mobility by people with spinal cord injury,"

Disability and Rehabilitation: Assistive Technology, vol. 11, pp. 535–547, Sept. 2015.

[21] A. E. Palermo, J. L. Maher, C. B. Baunsgaard, and M. S. Nash, "Clinician-focused overview of bionic exoskeleton use after spinal cord injury," *Topics in Spinal Cord Injury Rehabilitation*, vol. 23, pp. 234–244, June 2017.

[22] S. Lal, "Premature degenerative shoulder changes in spinal cord injury patients," *Spinal cord*, vol. 36, no. 3, pp. 186–189, 1998.

[23] W. Pentland and L. Twomey, "Upper limb function in persons with long term paraplegia and implications for independence: Part i," *Spinal Cord*, vol. 32, no. 4, pp. 211–218, 1994.

[24] L. L. Haubert, D. D. Gutierrez, C. J. Newsam, J. K. Gronley, S. J. Mulroy, and J. Perry, "A comparison of shoulder joint forces during ambulation with crutches versus a walker in persons with incomplete spinal cord injury," *Archives of Physical Medicine and Rehabilitation*, vol. 87, no. 1, pp. 63–70, 2006.

[25] A. F. Soliman and B. Ugurlu, "Robust locomotion control of a self-balancing and underactuated bipedal exoskeleton: Task prioritization and feedback control," *IEEE Robotics and Automation Letters*, vol. 6, pp. 5626–5633, May 2021.

[26] B. Ugurlu, C. Doppmann, M. Hamaya, P. Forni, T. Teramae, T. Noda, and J. Morimoto, "Variable ankle stiffness improves balance control: Experiments on a bipedal exoskeleton," *IEEE/ASME Transactions on Mechatronics*, vol. 21, pp. 79–87, Oct. 2017.

[27] H. Kawamoto, S. Taal, H. Niniss, T. Hayashi, K. Kamibayashi, K. Eguchi, and Y. Sankai, "Voluntary motion support control of robot suit hal triggered by bioelectrical signal for hemiplegia," in *Annual International Conference of the IEEE Engineering in Medicine and Biology*, pp. 462–466, 2010.

[28] S. Wang, L. Wang, C. Meijneke, E. van Asseldonk, T. Hoellinger, G. Cheron, Y. Ivanenko, V. L. Scaleia, F. Sylos-Labini, M. Molinari, F. Tamburella, I. Pisotta, F. Thorsteinsson, M. Ilzkovitz, J. Gancet, Y. Nevatia, R. Hauffe, F. Zanow, and H. van der Kooij, "Design and control of the MINDWALKER exoskeleton," *IEEE Transactions on Neural Systems and Rehabilitation Engineering*, vol. 23, pp. 277–286, Mar. 2015.

[29] M. C. Yildirim, A. T. Kansizoglu, S. Emre, M. Derman, S. Coruk, A. F. Soliman, P. Sendur, and B. Ugurlu, "Co-ex: A torque-controllable lower body exoskeleton for dependable human-robot co-existence," in *IEEE 16th International Conference on Rehabilitation Robotics (ICORR)*, IEEE, June 2019.

[30] C. Meijneke, G. van Oort, V. Sluiter, E. van Asseldonk, N. L. Tagliamonte, F. Tamburella, I. Pisotta, M. Masciullo, M. Arquilla, M. Molinari, A. R. Wu, F. Dzeladini, A. J. Ijspeert, and H. van der Kooij, "Symbitron exoskeleton:

Design, control, and evaluation of a modular exoskeleton for incomplete and complete spinal cord injured individuals," *IEEE Transactions on Neural Systems and Rehabilitation Engineering*, vol. 29, pp. 330–339, 2021.

[31] A. Agrawal, O. Harib, A. Hereid, S. Finet, M. Masselin, L. Praly, A. D. Ames, K. Sreenath, and J. W. Grizzle, "First steps towards translating HZD control of bipedal robots to decentralized control of exoskeletons," *IEEE Access*, vol. 5, pp. 9919–9934, 2017.

[32] G. Barbareschi, R. Richards, M. Thornton, T. Carlson, and C. Holloway, "Statically vs dynamically balanced gait: Analysis of a robotic exoskeleton compared with a human," in *37th Annual International Conference of the IEEE Engineering in Medicine and Biology Society (EMBC)*, IEEE, Aug. 2015.

[33] F. Mo, Q. Zhang, H. Zhang, J. Long, Y. Wang, G. Chen, and J. Ye, "A simulation-based framework with a proprioceptive musculoskeletal model for evaluating the rehabilitation exoskeleton system," *Computer Methods and Programs in Biomedicine*, vol. 208, p. 106270, 2021.

[34] H. Sadeghi, P. Allard, F. Prince, and H. Labelle, "Symmetry and limb dominance in able-bodied gait: a review," *Gait & Posture*, vol. 12, pp. 34–45, Sept. 2000.

[35] A. Roaas and G. B. J. Andersson, "Normal range of motion of the hip, knee and ankle joints in male subjects, 30–40 years of age," *Acta Orthopaedica Scandinavica*, vol. 53, pp. 205–208, Jan. 1982.

[36] B. Ugurlu, M. Acer, D. E. Barkana, I. Gocek, A. Kucukyilmaz, Y. Z. Arslan, H. Basturk, E. Samur, E. Ugur, R. Unal, and O. Bebek, "A soft+rigid hybrid exoskeleton concept in scissors-pendulum mode: A suit for human state sensing and an exoskeleton for assistance," in *IEEE 16th International Conference on Rehabilitation Robotics (ICORR)*, IEEE, June 2019.

[37] M. C. Yildirim, P. Sendur, A. T. Kansizoglu, U. Uras, O. Bilgin, S. Emre, G. G. Yapici, M. Arik, and B. Ugurlu, "Design and development of a durable series elastic actuator with an optimized spring topology," *Proc. IMECHe, Part C: Journal of Mechanical Engineering Science*, vol. 235, pp. 7848–7858, Oct. 2021.

[38] A. D. Santis, B. Siciliano, A. D. Luca, and A. Bicchi, "An atlas of physical human–robot interaction," *Mechanism and Machine Theory*, vol. 43, pp. 253–270, Mar. 2008.

[39] R. Budynas, J. Nisbett, and J. Shigley, *Shigley's mechanical engineering design. 9th ed.* New York: McGraw-Hill, 2011.

[40] D. W. Robinson, *Design and analysis of series elasticity in closed-loop actuator force control.* PhD thesis, Massachusetts Institute of Technology. Dept. of Mechanical Engineering, 2000.

[41] J. Pratt, B. Krupp, and C. Morse, "Series elastic actuators for high fidelity force control," *Industrial Robot: An International Journal*, vol. 29, no. 3, pp. 234–241, 2002.

[42] N. Paine, S. Oh, and L. Sentis, "Design and control considerations for high-performance series elastic actuators," *IEEE/ASME Transactions on Mechatronics*, vol. 19, no. 3, pp. 1080–1091, 2013.

[43] K. Kong, J. Bae, and M. Tomizuka, "A compact rotary series elastic actuator for human assistive systems," *IEEE/ASME Transactions on Mechatronics*, vol. 17, no. 2, pp. 288–297, 2011.

[44] E. J. Rouse, L. M. Mooney, E. C. Martinez-Villalpando, and H. M. Herr, "Clutchable series-elastic actuator: Design of a robotic knee prosthesis for minimum energy consumption," in *IEEE 13th International Conference on Rehabilitation Robotics (ICORR)*, pp. 1–6, IEEE, 2013.

[45] A. T. Kansizoglu, E. Sariyildiz, and B. Ugurlu, "A comparison study on observer-based force control of series elastic actuators," in *IEEE 15th International Workshop on Advanced Motion Control (AMC)*, pp. 411–416, 2018.

[46] E. Sariyildiz, R. Oboe, and K. Ohnishi, "Disturbance observer-based robust control and its applications: 35th anniversary overview," *IEEE Transactions on Industrial Electronics*, vol. 67, no. 3, pp. 2042–2053, 2020.

[47] G. Pratt, P. Willisson, C. Bolton, and A. Hofman, "Late motor processing in low-impedance robots: impedance control of series-elastic actuators," in *Proceedings of the American Control Conference*, vol. 4, pp. 3245–3251 vol.4, 2004.

[48] P. Tomei, "A simple pd controller for robots with elastic joints," *IEEE Transactions on Automatic Control*, vol. 36, no. 10, pp. 1208–1213, 1991.

[49] G. Wyeth, "Control issues for velocity sourced series elastic actuators," in *Proceedings of the Australasian Conference on Robotics and Automation*, pp. 1–6, Australian Robotics and Automation Association, 2006.

[50] H. Vallery, R. Ekkelenkamp, H. van der Kooij, and M. Buss, "Passive and accurate torque control of series elastic actuators," in *IEEE/RSJ International Conference on Intelligent Robots and Systems*, pp. 3534–3538, 2007.

[51] B. Ugurlu, E. Sariyildiz, A. T. Kansizoglu, E. C. Ozcinar, and S. Coruk, "Benchmarking torque control strategies for a torsion-based series elastic actuator," *IEEE Robotics and Automation Magazine*, vol. 29, no. 2, pp. 85–96, 2022.

[52] S. Oh and K. Kong, "High-precision robust force control of a series elastic actuator," *IEEE/ASME Transactions on Mechatronics*, vol. 22, no. 1, pp. 71–80, 2017.

[53] T. Ji and A. Pachi, "Frequency and velocity of people walking," *Struct. Eng*, vol. 84, no. 3, pp. 36–40, 2005.

[54] J. Hwangbo, J. Lee, and M. Hutter, "Per-contact iteration method for solving contact dynamics," *IEEE Robotics and Automation Letters*, vol. 3, no. 2, pp. 895–902, 2018.

[55] M. Vukobratović and B. Borovac, "Zero-moment point—thirty five years of its life," *International Journal of Humanoid Robotics*, vol. 1, no. 01, pp. 157–173, 2004.

[56] B. Ugurlu, I. Havoutis, C. Semini, K. Kayamori, D. G. Caldwell, and T. Narikiyo, "Pattern generation and compliant feedback control for quadrupedal dynamic trot-walking locomotion: experiments on robocat-1 and hyq," *Autonomous Robots*, vol. 38, no. 4, pp. 415–437, 2015.

[57] B. Ugurlu and A. Kawamura, "Bipedal walking trajectory generation based on zmp and euler's equations of motion," in *10th IEEE-RAS International Conference on Humanoid Robots*, pp. 468–473, 2010.

[58] S. Kajita, T. Nagasaki, K. Kaneko, and H. Hirukawa, "Zmp-based biped running control," *IEEE robotics & automation magazine*, vol. 14, no. 2, pp. 63–72, 2007.

[59] B. Ugurlu, J. A. Saglia, N. G. Tsagarakis, S. Morfey, and D. G. Caldwell, "Bipedal hopping pattern generation for passively compliant humanoids: Exploiting the resonance," *IEEE Transactions on Industrial Electronics*, vol. 61, no. 10, pp. 5431–5443, 2014.

VITA

Mustafa Derman graduated from Bornova Anatolian High School and started his Bachelor's Degree at Özyeğin University Mechanical Engineering in 2015. He worked in OZU Rover Team for 2 years and led the team in ERC2018 competition. He worked as an undergraduate research student for 2 years at Özyeğin University Biomechatronics Laboratory with Asst. Prof. Barkan Uğurlu. After graduating from his BSc in 2020, he started his master studies at Özyeğin University. He is studying robotics, human-robot interaction and control systems.